Faculty of Civil Engineering and Geosciences

Reconfigurable Modularity for shell structures

by

Sil Negenman

To obtain the degree of Master of Science
at the Delft University of Technology,
to be defended publicly on Wednesday July 16, 2025.

Student number: 4960254

Thesis committee:

	Prof.dr.ir Max Hendriks,	TU Delft
	Dr. Mariana Popescu,	TU Delft
	Dr. Robin Oval,	TU Delft / ENPC

TU Delft Delft University of Technology

Abstract

The building sector is a big sector that is very important for the global economy, but also has a big contribution to the greenhouse gas emission and production of construction waste. The building sector is responsible for about 37% of the global greenhouse gas emissions. In order to comply with the Paris Agreement on climate change, it is necessary to reduce the total emission of greenhouse gasses and the production of waste.
Modular construction is used for structural components, such as columns ,beams, and plates. However, it has not yet been implemented for shell structures. Shell structures are shape and material efficient, but often require unique formwork that is of one time usage, because of their complex geometries.

This research searches to improve the sustainability of shell structures by looking into the application of modular construction in this type of structures. With the use of the Goldberg-method a hexagon dominant pattern has been projected on a spherical dome structure. Creating a repeatable mesh pattern on the structural surface. Various segment sizes (N=4 till N=10) have been evaluated at the hand of a structural analysis in Grasshopper and Karamba3D. An uniform load, and a wind load have been used to obtain the stress distribution, displacement and buckling load factors for the different segment sizes.

It was found that smaller segments result in a more efficient force distribution, but larger segments have a lower labour intensity. From the analysis the optimal situation has been found at N=8, giving a balanced result between structural performance and labour intensity. With situation the difference in performance for different boundary conditions, and joint stiffness has been investigated. Here it was found that the segmentation of the shell lowers the buckling stability of a structure, but that modular construction is possible with different boundary conditions and even with the introduction of an oculus.
From the optimal situation N=8, 20 modules can be extracted. With the use of k-means clustering on the edges off the different modules, these modules can be further optimised. This leads to a adjusted set of 16 modules, with only 6 different module edges. The optimised modules have a higher potential for more configurations.

The results show that modular construction is possible within shell structures without compromising the structural integrity. It also results in a set of modules that can potentially be used in different configurations and across different structures. With this the research contributes to a more sustainable and circular construction approach for shell structures.

Acknowledgements

I want to thank my thesis committee for their support and advice throughout this thesis. I want to give a special thanks to Dr. Robin Oval for fulfilling the position of chair during the largest part of this thesis and for his continued support after transitioning to a different university. I also would like to thank Prof.dr.ir. Max Hendriks for stepping into the role of chair for the last part of this thesis, and Dr. Mariana Popescu for attending the meetings despite regularly being in a different location.

Content

List of Figures

List of Tables

1. Introduction

1.1. Research context

The building sector is a big sector that is very important for the global economy, but also has a big contribution to the greenhouse gas emission and production of construction waste. The building sector is responsible for about 37% of the global greenhouse gas emissions. (UNEP, 2022) And in the Netherlands alone, this sector produced 87 million kilograms of construction waste in 2016. (Berkel et al., 2019) In order to comply with the Paris Agreement on climate change, it is necessary to reduce the total emission of greenhouse gasses and the production of waste.

There are multiple ways to improve the sustainability of the construction sector over its multiple stages, such as the design, production, and the construction stage. One of the techniques used to reduce the environmental impact is the use of prefabricated (prefab) elements. With prefab elements, the construction process as well as the material usage, and the quality of the elements can be better monitored. With this the efficiency of the construction process and the material usage is more optimal, leading to less energy consumption and less material usage. (BouwWereld, 2025) (iBouw, 2025) There is also a limitation of different sizes of elements for prefab construction. The consequence is that in the design process, standard dimensions need to be considered for beams, columns, and plates. However, this also provides the opportunity to reuse and repurpose those elements after deconstruction if the design allows for that. In this case the modular prefab approach also contributes to a circular economy. (Fernhout, 2025)

A field where modular construction lacs behind is in the construction of shell structures. Shell structures are shape efficient structures, curved in such a way that they allow for a very efficient use of material. This leads to a thin shell, with structural efficiency and esthetical value. They can be used to cover large spans with minimal use of material. But because of the complex shapes they form to achieve the material efficient shapes, they also need very specific formwork for each element to be constructed. The differences between shell structures as well as the different curvatures within the same shell structure are illustrated in Figure 1. These wide range of shapes and curvatures lead to challenges in the sustainability of shell structures.

Figure 1: Bosjes chapel, South Afrika (left), Il Ponte sul Basento (middle) and Forest of meditation, Kakamiaahara, Japan (right) (Archello, 2024) (Shakeri, 2022) (Tumblr, 2009)

The formwork used to create the shell segments can be made from various materials. The traditional formwork is often constructed out of wood or metal, of which wood is the most commonly used formwork type. (Li et al., 2022) Wood has multiple advantages over other materials, namely being relatively light weight, can be cut into different shapes, and can be bend in the desired curvature. (Das et al., 2016) The disadvantage of wood is that it has a relatively low life span, which leads to a limited reusability of the formworks. (Gaddam et al., 2020)
Another formwork system is flexible formworks, like fabric, and pneumatic formwork. These type of formworks are more flexible and can more easily create non-standard geometries, while they also reduce the amount of material used in formwork, and the labour costs. (Li et al., 2022)

Research has been done to more sustainable formwork. A couple of examples for different approaches are reconfigurable formwork, wax formwork, and reusable knitted formwork. The research

of Kontovourkis yielded a reconfigurable modular formwork design, with which multiple module shapes can be created with a limited amount of different formwork. (Kontovourkis et al.,2019) The wax formwork was investigated by Oesterle. In his research the formwork is made with wax that can be remelted and reshaped in an easy way. This provides more possibilities for shape adaptation, while minimizing the material usage for the formwork. (Oesterle et al, 2012)

The improvement of formwork efficiency is a good step towards more sustainable shell structures. However, the challenge of the large variety of curvatures and shapes within shell structures remain. To solve this it would be better if shell structures were constructed in such a way that shell modules can be produced and used in a variety of shell structures. For this a trade-off needs to be made between structural performance and material efficiency.
This research will look into the use of modular design in the field of shell structures as well as a way to reduce the amount of unique shell segments. With this the environmental impact of shell structures can be reduced.

1.2 Problem statement and research objectives

The construction sector has a large climate impact and modular construction is one way to reduce this impact. So far this method has mainly been used for beams, columns, and plates, but not for shell structures. Although shell structures themselves are material efficient structures, they also produce a lot of construction waste because of the unique formwork that is needed for each shell structure.
Modular design as is used for beams, columns, and slaps can improve the sustainability, and reusability of shell structures. This leads to the research question formulated below:

- How can modular design be used in shell structures?

There are multiple steps needed to come to a conclusion for the research question above. Therefore the following sub-questions will be investigated as well:

- What module shapes can be selected for a modular construction?
- What radius of curvature can be used for the design?
- What would be the optimal size of the modules?
- What is the influence on the structural behaviour when modular construction is used for shell structures?
- What set of modules can be used to describe a variety of shell structures?

1.3 Scope

This thesis aims for a better understanding of the influence of modular constructure for shell structures. To achieve this, research will be done to the geometry of the module, as well as to the selection of a feasible curvature and size. To gain insight into the scale in which shell structures are created, and to select a relevant curvature for this research, a case study will be done into different kind of shell structures. There are different possibilities for the direction of the curvature, but in this research a spherical shape will be investigated. For the size of the modules, different sizes will be compared in a structural analysis. From this a module size will be chosen and used for further investigation of the structural behaviour. Other parameters that will be investigated are the stiffness of the joints and boundary conditions.
Once a set of modules has been found, further optimisation of the shape will be explored leading to a more diverse set of modules.

This thesis will not go into a design for the formwork of the shell modules, nor will it include calculations for potential reinforcement inside the modules. For the connections between the

modules, a strength and stiffness will be assumed, without detailed calculations. This way the focus remains on the structural behaviour of the entire dome and the finding of the module shapes.

1.4 Methods

To answer the research questions as described above, multiple methods will be used. In figure 2 the different steps in this report are displayed in the blue boxes. The orange circles display the methods used in the displayed steps.
To determine which geometrical shape is suitable for the module design, a literature review is conducted. In this review geometrical shapes and tiling patterns are evaluated.
In shell structures a lot of different shapes and curvatures are possible. Therefore one curvature needs to be chosen for the design. This design curvature is chosen with the use of a case study, looking into multiple shell structures and their shape. Then the literature review is continued with methods for dividing a structure into modules.
After the model is assembled, a structural analysis will be conducted to evaluate the structural behaviour for different module sizes, and boundary conditions.
Based on the structural analysis a set of modules will be extracted and optimized by using k-means clustering.

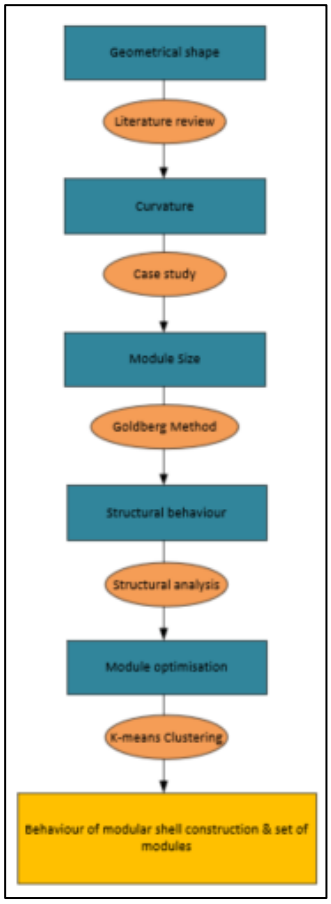

Figure 2: Thesis workflow.

1.5 Thesis structure

The structure of this thesis will be as follows: In chapter 2 a literature review will be conducted. In this review different tiling patterns, geometrical shapes, shell curvature, dome dimensions, and module design will be covered.
Then in chapter 3, the design choices for the geometrical shape, shell curvature, and other design specification will be explained.
In chapter 4, the structural model is assembled based on the design decisions from chapter 3, and the structural analysis will be performed.
After the structural analysis a set of modules will be created in chapter 5. These modules will then be further optimised using k-means clustering to improve the possibility of different configurations.
In chapter 6 the results of chapter 5 will be discussed in more detail, and finally the conclussions and recommendations will be given in chapter 7.

2. Literature review

This chapter will discuss the literature review. At first, ways to divide a surface are discussed in 2.1 followed by the properties of different geometrical shapes in 2.2. Then in 2.3 reference structures are selected to get a reference for an usable radius of curvature. In 2.4 useful formulas and rules are given for the design of an 'optimal' dome. A search for the amount of different modules to be used as well as methods for module creation are discussed in 2.5. Lastly useful software and tools will be discussed in section 2.6.

2.1 Tiling patterns

In modular construction, modules can connect to one another to form a complete structure. This can be done by splitting the surface of a shell structure in any given way and connecting the created segments to one another. However, in this way it is very unlikely that the segments can be used in different structures, which would undermine the purpose of modular construction as described in section 1.2. So the to be designed shell modules should be designed with a more general shape, in order for them to be usable in more than one way.

In theory any repeatable shape can be used to tessellate a surface. However, complicated shapes will also complicate the design and therefore it is easier to use basic shapes. Different ways in which basic shapes can be used to tessellate a surface are described with Archimedean tiling patterns. Figure 3 showcases these patterns, where the large numbers underneath each configuration describe the basic shape and the smaller number describes the amount of shapes connecting in the corners.

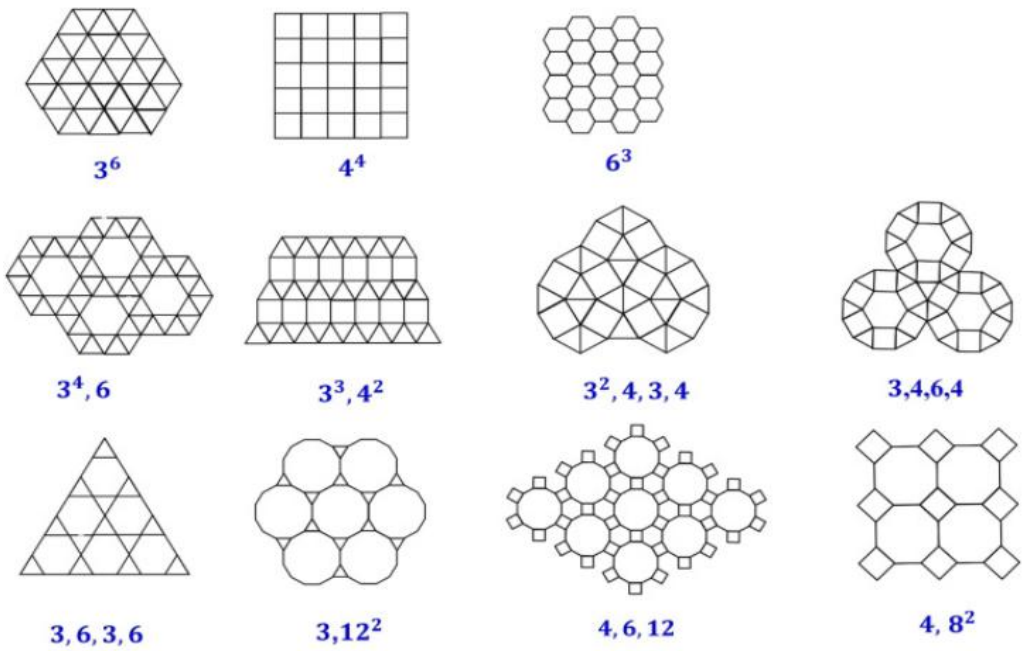

Figure 3: Archimedean tiling patterns (Kuo S., 2023)

The first three patterns consist of only one type of polygon and are called regular Archimedean tiling's. The polygons used in these patterns are the triangle, square, and hexagon and are the only three polygons that can tessellate a surface with one shape. Other polygons can also be used in a pattern, as can be seen in the remaining patterns in Figure 3**Fout! Verwijzingsbron niet gevonden.**, but then they need to be combined with other polygons to completely fill a surface. These patterns are the irregular Archimedean tiling's. (Kuo S., 2023)

There are also other patterns besides the Archimedean tiling patterns, such as the Penrose tiling (Javan et al, 2024) and the Escher tiling's (Howson et al, 2009). Eventhough these patterns are also very interesting, their unique shape will also complicate both the design and the construction.

It is important to notice that the patterns in the figure above are describing flat surfaces, but the shapes used in theses patterns can also be used in a 3D setting. Often the three basic shapes of triangle, square and hexagon can be seen in geodesic domes. (Rasheed et al, 2015) (Guan et al, 2018) However, it does not have to consist of only one size of polygon. (Dede et al, 2022)

In the case of a geodesic dome the polygons are not all exactly equal. They need to deform a little bit, depending on their place on the structure, to completely fill up the surface. In order to use only one size for a polygon, the Archimedean tiling patterns need to be extended to a 3D application. In case one specific shape is repeated to form a 3D shape, it is called a platonic solid. In Figure 4 **Fout! Verwijzingsbron niet gevonden.**the different platonic solids are displayed. It can be noticed that the triangle and the square, which were also present in the regular Archimedean tiling patterns, return, but that the hexagon is not there. Instead there is the dodecahedron consisting of pentagons. It can also be noticed that the platonic solids start to describe a curved surface better with more polygons in their design.

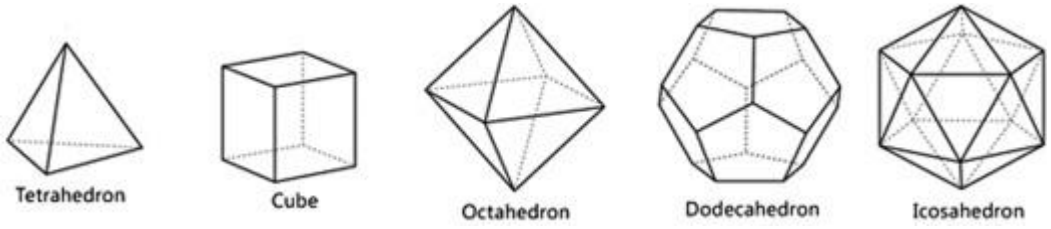

Figure 4: Platonic Solids (Datta et al, 2022)

Configurations with multiple types of polygons are called the Archimedean solids. In Figure 5 the Archimedean solids are displayed. The advantage over the platonic Solids is that in general they more closely resemble a sphere. This is useful when the shapes are used to create a curved surface. The downside is that there are multiple types of polygons needed to create the solids. In the search for a limited set of shell modules, different types of polygons in the design will automatically lead to more unique modules. The Archimedean solids can nonetheless be a useful configuration.

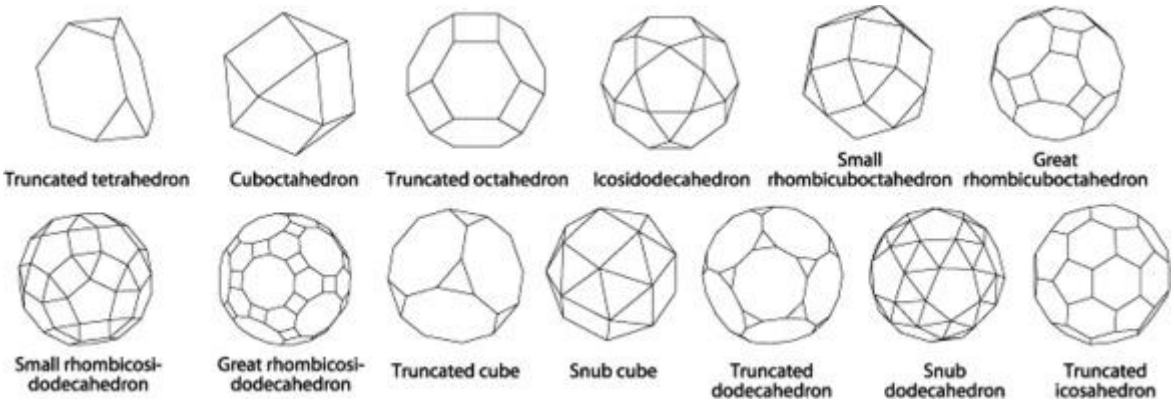

Figure 5: Archimedean solids (Datta et al, 2022)

When the Archimedean tiling's are applied on a curved surface in multiple directions, often some sort of mapping is used. This leads to slight deformation of the original polygons. A type of pattern that deliberately uses this is a Voronoi pattern and it can make for a strong and lightweight structure. (Dong et al, 2024) The pattern is inspired by observations in nature, where this pattern can be found in metals (van Nuland et al, 2021), ceramics (Coster et al, 2002), honeycombs and the wings of a dragonfly. (Gawell et al, 2015)
Although the Voronoi pattern makes for a strong and efficient structure, it does not provide a clearly repeatable pattern, which is needed to design a limited set of modules.

2.2 Geometrical shape

The tiling patterns found above show that there are multiple combinations of polygons possible. However, in geodesic domes often either triangles, squares, or hexagons are chosen. Different polygons have different properties. To decide on a governing shape for the module set, these properties will be investigated.

The triangular shape is considered to make the most statically efficient structure. This is because the triangular shape cannot deform without extension or compression of the polygon arms. (Tonnelli et al, 2016) For higher order polygons the connection between the arms can be the weak point of the polygon and then the polygon can deform without deformation of the arms.

Higher order polygons have a higher area/perimeter ratio. This ratio tells how much area the polygon encloses for every unit of perimeter length and is used as a comparison on how efficiently a shape encloses space. With a higher ratio it would mean that more area is encapsulated by the perimeter than it would be for a lower ratio. In general this minimizes material usage for enclosed area. (Birch et al, 2007). Another aspect is, that the higher the area/perimeter ratio is, the better the shape will be able to follow curved surface in a 'natural' way. (ArcGIS, 2024) So a high area/perimeter ratio can help with creating a smooth and natural appealing structure with limited material usage. And this will then lead to a cheaper production process. A downside of the higher order polygons is that they are less statically efficient than the triangular mesh and therefore often need an additional stability system, such as a bracing cable system. (Tonneli et al, 2016)

Depending on the shape of the segments a certain number of segments need to align in one point. For a triangular shape this can be up to 6 different segments. For a rectangular pattern 4 segments need to connect in one node, and for a hexagonal module this number is only 3. A node with lesser modules to connect is easier to design and easier to assemble. (Tonneli, 2015)
The Voronoi pattern that was described in the tiling patterns also mostly consist of hexagons. (Tellier, 2020)

2.3 Shell curvature

Another consideration for the module design is which curvature the modules should have to be representative for a variety of structures. For this, different shell structures are evaluated based on their shapes. The difficulty is that there are many possible curvatures for a shell structure, since the dimensions of each building are different. This difference is both in size and in shape and can even occur within one structure. This difference can be seen in blueprints found on the internet for different structures. One is the Bosjes chapel, South Afrika. (Stevens, 2017) Others are: the Heydar Aliyev centre in Azerbaijan, and L'oceanographic in Valencia. (archdaily, 2013) (Banos, 2024) These blueprints will be used for measuring the curvature at different places on the structures.

More easily measurable shell structures are dome constructions. However, usually only the diameter of the dome is given and not the radius of curvature. In Table 1 different domes with their found diameter are given.

Table 1: Diameter of different domes. (Britannica, 2024), (architecturecourses, 2024), (VisitVaticanCity, 2024), (Britannica, 2024), (Tajmahal.gov, 2024)

Dome	Pantheon	Hagia Sophia	St. Peter's Bsilica	Dome of the Rock	Taj Mahal
Diameter [m]	43	30	42	20	18

2.4 Dome mechanics

In the course CIEM5301 Shell structures, given at the TU Delft, an 'optimal' dome is described. Here the 'optimal' refers to the material usage in constructing the dome. Here it is given that a spherical cap of constant thickness has the optimal sagitta to span ratio of $\sqrt{3}$ over 6. This aspect can be used to calculate the radius of curvature of such a dome. The formula to get the radius of curvature is given below. (Hoogenboom, 2023)

$$R = \frac{s}{2} + \frac{d^2}{8s} \quad [1]$$

Where:

$R = Radius\ of\ curvature. [m]$
$s = The\ sagitta/height\ of\ the\ dome. [m]$
$d = The\ diameter\ of\ the\ domes\ base. [m]$

In general there are not many references that go into the optimal curvature of a shell. Each shell is formed in such a way that the form and curvatures in the structure are optimized for the boundary conditions of the specific structure. An exception on this is the research of A. S. Jape and A. S. Sayad. They investigated the displacements, stresses, and fundamental frequencies in shell segments with different radii of curvature. They concluded that the radii of curvature of 5 and 10m performed better when it comes to displacements and stresses in spherical, cylindrical, and elliptical shells than the radii 20, 50 and 100m. (Jape et al, 2023)

The curvature of a shell is one property, but for a complete structure the thickness of the shell also needs to be determined. The required thickness is dependent on the shape of the structure and the load on the structure. A type of structure where the thickness can be easily determined is the optimal dome as mentioned before. For a fully stressed dome, a thickness can be assumed based on the following formula: (Hoogenboom, 2025)

$$t = \frac{\sigma * R}{0.1 * E} \quad [2]$$

Where:

$t = thickness\ of\ the\ shell\ [mm]$

$\sigma = the\ stress\ \left[\frac{N}{mm^2}\right]$

$E = modulus\ of\ elasticity\ [\frac{N}{mm^2}]$

$R = radius\ of\ curvature\ [mm]$

The stresses that can be expected in a dome under self-weight can be calculated with formulas 3, and 4. Here formula 3 gives the meridional stress in the dome foot and formula 4 gives the meridional stress in the top of the dome. (Hoogenboom, 2025)

$$\sigma = 2 * \frac{R^2 \rho g}{l^2}\left(2R - \sqrt{4R^2 - l^2}\right) \quad [3]$$

$$\sigma = \frac{1}{2} R \rho g \quad [4]$$

Where:

$\sigma = the\ stress\ \left[\frac{N}{m^2}\right]$

$\rho = density\ of\ the\ dome\ material\ \left[\frac{kg}{m^3}\right]$

$g = grafitational\ force\ [m/s^2]$

$R = radius\ of\ curvature\ [m]$

$l = diameter\ of\ the\ dome\ base\ [m]$

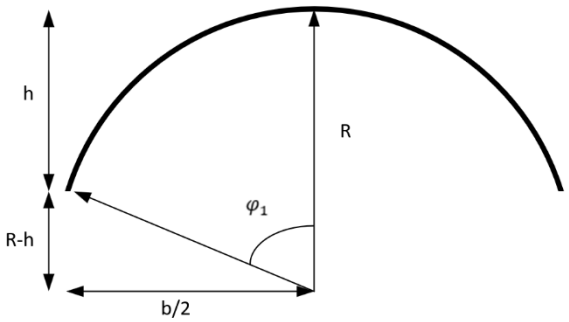

Figure 6: Geometry of a dome.

To calculate the deflection of the dome, formula 5 is used. (Ventsel&Krauthammer, 2001) In figure 6 the geometry of the dome is displayed, which is used to calculate variables in formula 5.

$$u = \frac{pR^2(1+\nu)}{Et}\sin(\varphi)\left[\ln\left(\frac{1+\cos(\varphi)}{1+\cos(\varphi_1)}\right) + \frac{\cos(\varphi)-\cos(\varphi_1)}{(1+\cos(\varphi))(1+\cos(\varphi_1))}\right] \quad [5]$$

Where:
p = (uniform) load on the structure [kN/m^2]
R = Radius of curvature [m]
ν = viscosity [-]
E = Modulus of elasticity [kN/m^2]
t = Shell thickness [m]
φ = angle from the dome top to point on structure [deg]
φ_1 = angle from the dome base to the top [deg]

2.5 Amount of modules

For the amount of modules that are needed to tessellate a curved surface, there is no clear answer. In the research of Mahroo and Vafamehr four modules have been created for a roof construction. However, other than the mentioning of using form finding in the modelling, there is no mention of why the amount of 4 modules was chosen. (Mahroo et al, 2023)
Another research is the one of De Coster et al, where they used a set of four shell modules of which two are triangular and two rectangular. However, this report mainly focuses on the configuration of the modules and does not mention the design of the modules. (De Coster et al, 2024)
A third research that has been found is the research of Kontovourkis et al. This research is more focused on the formwork of modules. They were able to create a reusable formwork in which they could adjust the shape a bit in order to create different modules. The amount of different modules they designed was 308 modules with only 15 sets of formwork. (Kontovourkis et al, 2019)

Other researches use k-means clustering to optimize the design. The research of J. Zhu used this method to optimize the structure on cost, quality and carbon emissions, showing that k-means clustering can be used as an optimization tool. (Zhu, 2024)
The research of Y. Liu et al used clustering-optimization in a framework to reduce the number of different nodes in space frames. (Liu et al, 2023) Another research using K-means clustering is the research of Keith Lee et all. They used clustering on nodes in a spatial truss and used forces inside the construction members as their clustering criteria. (Lee et al, 2022)

For a concrete amount of modules that is needed to tessellate a surface, not much information can be found. In general there can be different kind of curved surfaces. The first kind is a flat module and will be the simplest to produce. Another type is a module curved in one direction. Then for modules

curved in two directions there are two different kinds. A double curved surface can be synclastic and anticlastic.

The size of the modules will also influence how many modules are needed to cover a surface. The bigger the modules, the more area is covered with one module and the less modules are needed. However, big modules are also heavier and more difficult to handle during construction. With smaller modules, less heavy machinery is needed, but there will be more elements to put into place. Besides these considerations, also the transportation of the modules needs to be taken into account. In general prefabricated plates come in a maximum size of 200x200cm or 200x300cm. (Constar, 2024), (De Keij, 2024), (Jongeneel, 2024)
These dimensions are likely based on the dimensions of an average truck. The maximum width a vehicle can have is determined to be 2.5m in width. (85/3/EEC, 1984) Most trucks however are slightly smaller than this, around 2.45-2.48m. (BTA-international, 2024) The dimensions of the modules should fit within this dimension. Bigger is also possible, but then special vehicles must be used and special permission is needed before transportation.

2.6 Software and tools

Although the researches from section 2.4 did not include an explanation about the amount of modules, they did mention the software that was used to come to the results. They all worked in Rhinoceros and Grasshopper using various plug-ins. Kangaroo 2 is often used for form-finding, Lunchbox and Weaverbird for mesh creation, and Millipede, Ameba, and Galapagos for parametric design and optimization. (Mahroo et al, 2023), (De Coster et al, 2024) (Kontovourkis et al, 2019)

The Goldberg method is a method that can be used to create high symmetry in a structure. This method is explored by Rasheed et al and Liu et all. The method includes using platonic solids to represent a structure. The symmetric faces of this platonic solid can then be used to map a pattern onto it. This pattern is then transferred to the curved surface, leading to a symmetric design with a limited amount of modules. (Rasheed et al, 2015), (Liu et al, 2022)

3. Design specifications

This chapter will dive into the design specifications of the shell modules. First the design choice for the dominant module shape will be discussed in section 3.1. Then the curvature the design will be based on will be selected in section 3.2, based on a case study on different shell structures. In section 3.3 the material choice and corresponding shell thickness will be decided on. With the found dimensions and properties, two load cases will be determined in section 3.4. Lastly expected values for the stresses and deformation in the structure will be calculated in section 3.5.

3.1 General module shape

The goal of this research is to investigate the behaviour of shell structures when modular construction is applied. For this the surface will be split up in different segments. The amount of different segments needs to be limited in order to keep the amount of formwork needed for construction as low as possible. Therefore a general shape of the modules needs to be selected, since multiple shapes will automatically lead to more different formworks and increase the material usage.

In the literature review it was found that there are three polygons that are able to tessellate a flat surface without needing any other type of polygon. These were the triangle, rectangle and hexagon. On a 3D surface there will be some deformation of the flat patterns, but the deformed polygons will still be more similar to one another than would be the case between different kind of polygons. From these three polygons the hexagon has the highest area/perimeter ratio. This means that there is more area within the modules that have potential for further material optimisation. With the other polygons this is also possible, but the impact would not be as big, because the area/perimeter ratio is lower. Other possibilities would be to use infill panels to increase insulation, material combinations for lightweight structures, or transparent infill for natural light in the structure. With these options both the environmental impact as well as the construction costs can be further reduced. In this research these options will not be implemented, but it is good to keep these aspects in mind for possible future optimisation.

Another advantage of the hexagonal shape over the triangle or rectangle is that the connections between different modules only have to connect three modules. This makes for an easier construction and design of the connections in case of connections in the module nodes. The hexagon also has more sides than the triangle and rectangle, since it is a higher order polygon. This increases the possibility of reconfigurability, since it simply has more sides to connect to another module. With more configurations the modules will have a bigger change of describing a larger variety of structures.

So for the shape design of the modules a hexagonal dominant mesh will be used. Even though the hexagonal shape will be the governing shape used in the tiling pattern, it will not exclude other polygons. The Goldberg method mentioned in section 2.5 uses a repeatable pattern on multiple surfaces. The way these surfaces connect depends on the surfaces itself and the way the pattern is oriented in this. So it is still possible that other polygons will come out alongside the dominant hexagonal pattern.

3.2. Shell curvature

Not only the general shape of the modules is important, but also the curvature needs to be decided on. Because of the wide range of shapes shell structures are used for, there are still many possibilities for the curvature of the modules. In order to make a decision on the curvature of the modules, multiple existing shell structures are evaluated. Structures included in this evaluation are the Bosjes chapel, Heydar Aliyev centre, and Oceanographic. For these structures blueprints were found as was mentioned in the literature review. The blueprints were used to make measurements on various points on the structures. The results can be found in table 2.

The structures mentioned above have a shape that covers a variety of different curvatures. Structures that are more uniform are dome structures. In table 2 a variety of different dome structures has been listed. In the literature review the diameter of these domes were found. If it is assumed that the domes can be approximated by the principle of an 'optimal' dome, then they have a hight/diameter ratio of $\sqrt{3}/6$. This in combination with formula 1 leads to a formula for the radius of curvature as a function of the dome span. This can be found in formula 6 below:

$$R = \frac{\sqrt{3}}{3} * l \qquad [6]$$

With formula 6, table 2 can be completed by calculating the radius of curvature for each dome.

Table 2: Curvatures of existing shell structures.

Structure	**Diameter (m)**	**Radius of curvature (m)**
Pantheon	43	24.8
Hagia Sophia	30	17.3
St. Peter's Basilica	42	24.25
Dome of the Rock	20	11.5
Taj Mahal	17.68	10.2
Bosjes chapel	-	2.35
Heydar Aliyev centre	-	26.7 10 30 5 8 6.667
Oceanographic	-	3.1 6.2 14.97

In Table 2 can be seen that the radius of curvature is strongly dependent on the structure it is calculated for. However, the shell modules that are to be designed are meant to be able to describe a variety of different structures. Therefore the radius of curvature should be an average value, meaning that very large and very small radius of curvature should not be considered. This combined with the research of Jape et al, stating that smaller curvatures provide more stiffness, leads to a radius of curvature around 5 to 10m. Of these two 5m is in range with the smallest curvatures from table 2. This is rather small, so for the modules to be able to describe a larger variety of structures, while still providing sufficient stiffness, a radius of 10m is taken for this design.

For a shell structure the surface can curve in different directions. In general there are flat shapes, synclastic shapes, and anti-clastic shapes. For this design first a synclastic shape is considered, because a synclastic shape only curves in one direction, making it more easy to produce over an anti-clastic shape. And in order to put an anti-clastic shape into a structure, there needs to be a transition zone from one curvature to another. This leads to a variable radius of curvature, while for a synclastic shape the curvature never changes. The structure used to create the synclastic modules, and to investigate the change in structural behaviour with modular construction, is a dome structure.

3.3 Dome properties

In this section all properties and conditions for the dome structure used in the design are discussed. First the dimensions of the dome will be discussed.

Dome dimensions

The dimensions of the dome used for this project are based on the dimensions of an optimal dome as described in the literature review. Based on this, the dome dimensions can be calculated with formula 1 and with the given sagitta/span ratio of $\sqrt{3}/6$. From section 3.2 a radius of curvature of 10m was selected. With the given ratio of the dome and the radius of curvature the dimensions are given below:

$$R = \frac{s}{2} + \left(\frac{\left(\frac{6}{\sqrt{3}}s\right)^2}{8s} \right) = 2s \rightarrow s = \frac{1}{2}R = 5\ [m]$$

$$l = \frac{6}{\sqrt{3}}s = 17.31\ [m]$$

The material out of which the dome will be constructed will influence the thickness of the shell as well as the self-weight and material properties. For the creation of the shell modules concrete is selected as construction material. Concrete is a material that can be poured in any desired shape and that performs well under pressure. The optimal dome structure also allows for a good stress distribution, which makes that forces are not expected to be very high. Therefore a high strength material will not be necessary, and a more common material strength can be chosen. For this project material C20/25 will be taken.

For a fully stressed dome the buckling criteria can be used to calculate the required thickness of a dome. Formula 2 from the literature review can be used with a radius of curvature of 10m, modulus of elasticity of 30000 N/mm^2, and stress of $20/1.5 = 13.3\ N/mm^2$. For this formula it is assumed that the stress in the dome is governing for the structure. The stress in the dome should not exceed the stress at which buckling occurs. Filling in formula 2 gives:

$$13.3 \leq 0.1 * 30000 * \frac{t}{10000} \rightarrow t \geq 44\ [mm]$$

So the thickness of the shell must be more than 44mm. The thickness that will be used is 50mm.

Joints

The shell segments also need a way of connecting to one another. This will be done using a grout between the modules. With the grout gaps can be filled and some allowance for misalignments is introduced. This increases the possibility of different configurations, since the segments don't have to align perfectly.
The stiffness of the connections depends on the material that is used for the connections. There are different types of mortar with different material properties. Two common types of mortar are cement based and lime based. Both have their own advantages and disadvantages, but for this project cement mortar will be chosen. This is because cement mortar has in general a higher load-bearing capacity and is more weather resistant than lime mortar. Besides this, cement mortar is also less expensive. (VDMConstruction, 2025)

The material properties will also depend on the water/cement ratio. The research of Marques et al looked into the modulus of elasticity for different compositions of mortar. (Marques et al., 2020) For the application in the dome structure it is assumed that the mortar will have approximately the same strength as the shell segments. For this the mortar Ci_1:2 is taken as reference from the research of Marques et al. This brings a modulus of elasticity of around 25 Gpa.

For the rotational stiffness of the line joints, the joints are approximated as small elastic beams. The rotational stiffness can be calculated with the formula's (Skrinar et al, 2004):

$$K_r = M/\theta \quad [7]$$

Where θ can be calculated with:

$$\theta = \frac{M}{EI} * h \quad [8]$$

Leading to:

$$K_r = EI/h \quad [9]$$

The modulus of elasticity was determined to be 25000 Mpa. And I is the moment of inertia of the cross-section of the line joint. The height of the line joint is taken as the thickness of the shell segments, so 50mm. And the width of the cross-section is taken as the gap between two shell segments. This gap will depend on how closely the modules align to one another. It is assumed that there is a gap of 2cm between the different modules. This way it is taken into account that the modules do not have to align perfectly in different configurations, so some redundancy for misalignments is taken into consideration. So the value for the width of the cross-section is taken as 2cm. This leads to:

Kr = (25000000 * (0.02 * 0.05^3 /12))/0.05 = 104.2 kNm/m/rad

The supports at the boundary of the dome are assumed to be free in rotation, but fixed in x, y, and z direction.

Load cases

For the load combinations two different load cases are taken into account. The first load case is a uniformly distributed load and the second load case introduces an asymmetrical load situation. The two different load cases are determined below.

Uniform load:

For the load cases there is the self-weight of the structure. With the given thickness of 50mm, a mass of 2500 kg/m^3, and the gravitational force of 9.81 m/s^2 this gives:

$$t*\rho*g = 0.05*2500*9.81/1000 = 1.23 \text{ kN}/m^2 \quad [9]$$

For the variable load a snow load is considered as well as a load for maintenance work. The snow load is determined using formula 10. Here it is assumed that the structure is located in the Netherlands and that the dome has an average roof angle of 30 degrees.

$$s = \mu_i * C_e * C_t * s_k = 0.8 *1.0*1.0*0.7 = 0.56 \text{ kN}/m^2 \quad [10]$$

The variable load for maintenance work on roofs is given in the Quick reference as 1.0 kN/m^2. [Quick Reference, 2014]

With the loads found above there are three possible load combinations of which the one with the highest load will be taken as the governing load combination for the vertical loads. The snow load and the variable roof load are seen as two separate load combinations, because the snow load has a combination factor of 0. The load combinations are calculated below:

$$1.35 * G = 1.35 * 1.23 = 1.66 \text{ kN}/m^2$$

$$1.2 * G + 1.5 * Q_{snow} = 1.2 * 1.23 + 1.5 * 0.56 = 2.32 \text{ kN}/m^2$$

$$1.2 * G + 1.5 * Q_{variable} = 1.2 * 1.23 + 1.5 * 1.0 = 2.98 \text{ kN}/m^2$$

As can be seen above the load combination of the self-weight and the variable roof load is governing with a load of 2.98 kN/m^2.

Wind load:
The wind load against the dome can be calculated with the formula below.

$$Q_{wind} = C_{scd} * c_f * q_p(z_e) * A_{ref} \quad [11]$$

In order to fill in this formula, some assumptions need to be made. First it is assumed that the dome shape can be resembled by a duo pitched roof with an angle of approximately 30 degrees. For the location of the dome it is assumed that it is located in wind region 2 as defined in figure 7a, and build in a coastal area. And it will be assumed that the dome structure will be part of a larger structure and thus will be higher from the ground than the hight of the dome itself. The assumed height will be taken as 10m. This then leads to a value for qp(z=10)=1.32.

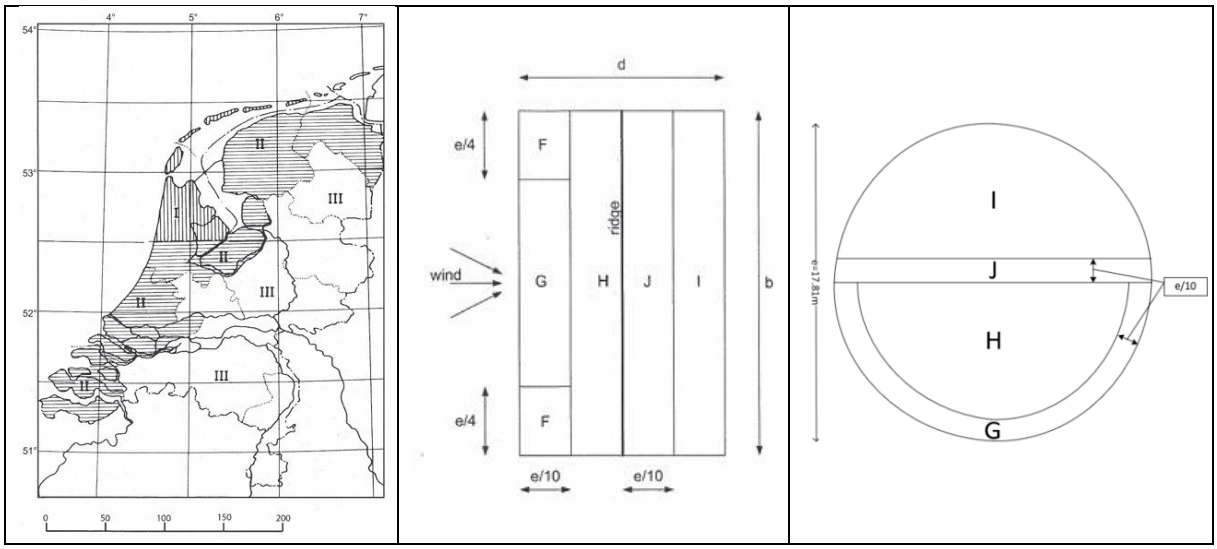

a) b) c)

Figure 7: Determination of wind zones. a) wind zones in the Netherlands. [QuickReference, 2014] b) Wind zones on a pitched roof. [QuickReference, 2014] c) Wind zones on a dome structure.

With the conditions as described above the factor c_f can be determined for each roof zone. In code NEN-EN 1991-1-4 there is no specific regulation for dome constructions, the values for c_f are taken for a shield roof. The different roof zones are determined at the hand of a double pitched roof which can be found in figure 7b. The middle of the dome is taken as the ridge and no corner zones are taken into account, since a circle does not have corners. The different roof zones are displayed in figure 7c. This leads to the numbers in the table below.

Table 3: Cf values according to NEN-EN 1991-1-4

	G	H	I	J
Cf [-]	-0.5 +0.7	-0.2 +0.4	-0.4 0	-0.7 0
Aref [m2]	42.36	75.31	87.7	29.96

The formula for the wind load calculates the total force on the structure. Therefore the resulting force will be divided by the total area of the structure to get a distributed load. The total area of the dome is a summation of the different zones and results in 235.33 m2. With the two different values for Cf, the two resulting wind loads are given below.

Q_{wind}= (1.0*1.32*(-0.5*42.36+-0.2*75.31+-0.4*87.7+-0.7*29.96))/235.33=-0.518 kN/m^2

Q_{wind}= (1.0*1.32*(0.7*42.36+0.4*75.31))/235.33=0.335 kN/m^2

From the two load situations above the load of 0.518 kN/m2 is governing. However, a safety factor should be applied on the load. With a safety factor for variable loads of 1.5, the design load becomes 1.5*0.518=0.777 kN/m2 and works in horizontal direction.
It is also assumed that when high wind loads occur, there will be no other variable loads than the wind load. From the uniform load only the permanent load remains, which was 1.23 kN/m2. And with a safety factor of 1.2 this value becomes 1.476 kN/m2 and works in vertical direction.

3.4 Expected outcomes

In order to make sure that the computer model will give the right results, it is important to know which values to expect. In section 2.3 several formulas were found for the deflection in a dome, and the stress in both top and bottom of a dome. In these formulas the dome is assumed to be a monolithic structure instead of a modular structure.
The formula for the deflection is dependent on the load, the radius of curvature, thickness of the shell, and the material properties. These were all determined in the earlier sections of this report. The only value still missing is the angle from top of the dome to the base of the dome. This can be calculated from the geometry of the dome as was displayed in figure 6. This leads to:

$$\varphi_1 = \tan^{-1}\left(\frac{\frac{b}{2}}{R-h}\right) = \tan^{-1}\left(\frac{\frac{17.31}{2}}{10-5}\right) = 59.98\ degrees$$

With this value for φ_1 formula 4 can be given as a function of φ and is given as:

$$u = \frac{0.00298 * 10^2(1+0.15)}{30000*5} * \sin(\varphi) * \left[\ln\left(\frac{1+\cos(\varphi)}{1+\cos(59.98)}\right) + \frac{\cos(\varphi)-\cos(59.98)}{(1+\cos(\varphi))(1+\cos(59.98))}\right]$$

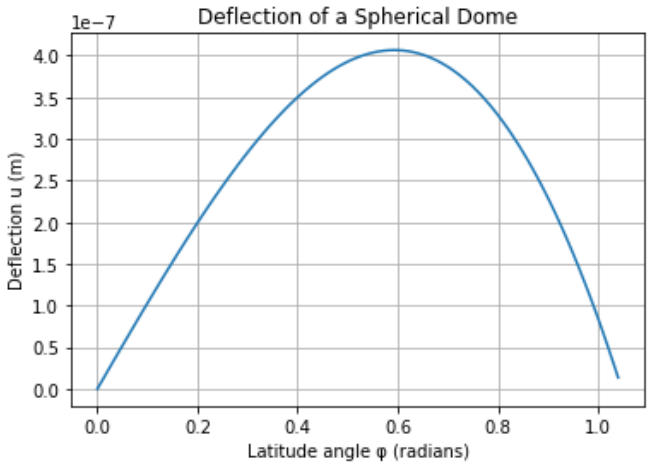

Figure 8: Deflection over the latitude angle along the dome.

In the figure 8 above, formula 12 is displayed and represents the accumulation of deflection in each point along the arch of the dome. To get the total deflection in the middle of the dome, the area under the graph should be taken and multiplied by the curvature of the dome. The area underneath the graph is determined with interpolation in python coding and gives a result of 0.0276 mm*rad. To get to the maximal deflection this result should be multiplied by the curvature, which is 1/10. So the deflection in the middle of the dome should be around 0.276 mm.

To calculate the expected stresses in the dome, formulas 3 and 4 are used. These formulas are for structures under self-load only, but the self-weight of the structure can be adjusted a bit to match the designed load of 2.98 kN/m^2. To adjust the load to the right format, it is set to 2980 N/m^2 and

divided by the thickness of the shell, which was 0.05m. Then the term $\rho * g$ can be replaced by this term. This leads to:

$$\sigma = 2 * \frac{10^2 * \frac{2980}{0.05}}{17.31^2}\left(2 * 10 - \sqrt{4 * 10^2 - 17.31^2}\right) * 10^{-6} = 0.397\ N/mm^2$$

$$\sigma = \frac{1}{2} * 10 * \frac{2980}{0.05} = 0.298\ N/mm^2$$

So a stress can be expected of approximately 0.297 N/mm^2 at the base of the dome, and approximately 0.298 N/mm^2 at the top of the dome. These values are for a monolythic dome, while the model will consist of multiple shell segments. Also the boundary conditions are assumed to be a continuous support, but some amount of lateral translation is allowed. If in the model the supports are assumed to be fixed, but free in rotation, this might cause some difference in outcome. However even though the assumptions of the hand calculation are not entirely the same as the model, the results should still be close to one another.

4. Structural Analysis

This chapter will discuss the steps and results of the structural analysis. In section 4.1 the creation of the different shell segments with the Goldberg method is discussed. From this a repeatable pattern comes forth, which will be used to create the structural model in Grasshopper. This will be covered in section 4.2. In section 4.3 the results of the structural analysis are given.

4.1 Goldberg method

For the mesh pattern and the module creation the Goldberg method is applied. This method is used because it leads to a high repeatability of shapes on a curved surface. This method consists of a couple of steps, which are listed below and visualized in figure 9.

1) Create a 2D tiling pattern consistent of hexagons.
2) Inside the 2D tiling pattern, draw a triangle with the dimensions n, m. Here n is the amount of hexagons that fit in the width of the triangle and m the amount of hexagons that fit in the height of the triangle.
3) Project the 2D tiling pattern inside the triangle
4) Create an icosahedron with the desired radius
5) Project the obtained mesh in step 3 on the icosahedron
6) Move every corner point of each polygon to the surface of a sphere.
7) Project the pattern onto the sphere to get the curved segments

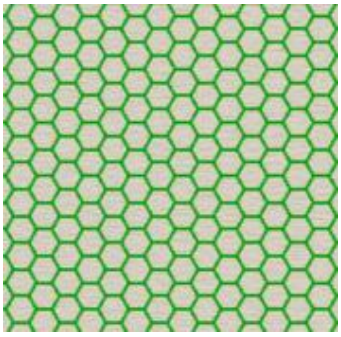

a)

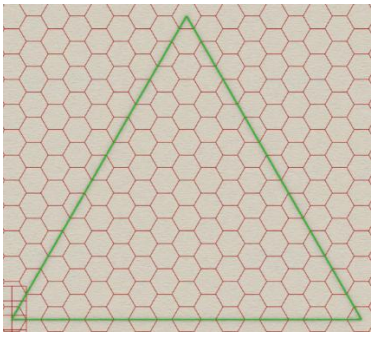

b)

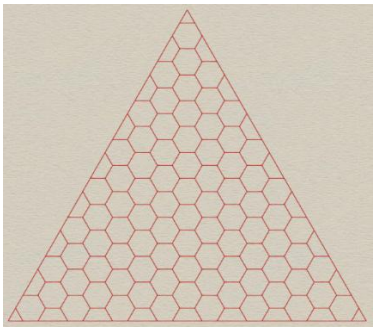

c)

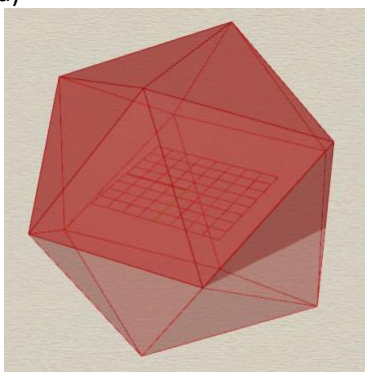

d)

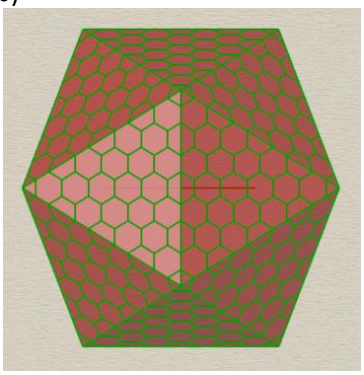

e)

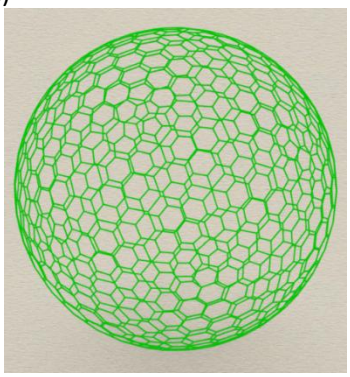

f)

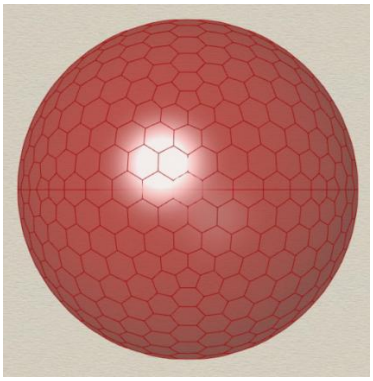

g)

Figure 9: Steps of the Goldberg method. 4.a) Creation of hexagonal mesh. 4.b) Drawing triangle in the mesh. 4.c) Projecting hexagons in triangle. 4.d) Icosahedron. 4.e) Project mesh on Icosahedron. 4.f) Transfer mesh to sphere 4.g) Full sphere

The 2D hexagonal pattern in step one will consist of hexagons of one shape and size. This will ensure a high repeatability in the following steps. The hexagonal mesh is projected on a triangle in steps 2 and 3. This leads to standard hexagons in the middle of the triangle, halves of the standard hexagon along the sides, and a sixths of the standard hexagon in the corners.
The icosahedron in step 4 is a platonic solid and is built up from equal triangles. This will ensure an equal projection of the hexagonal mesh in step 5. Because the corners of the icosahedron consist of five triangles coming together, this will automatically lead to a pentagonal shape in these corners. Along the edges there will be hexagons with a bend in the middle, since two halves of the standard hexagons are connected under an angle. The standard hexagons will not change in size.
To fit the pentagons and hexagons to a curved shape, the corner points of each polygon are moved to the closest point of the surface of a sphere. The corner points of the icosahedron are located on the sphere and the middle of each triangular surface is furthest away from the surface of the sphere. This will lead to an uneven distance for the different corner points of the polygons in the mesh and therefore, depending on that distance, the polygons will distort slightly differently. However, there is still a repeated pattern in the moved mesh, since the corner points of the most centred hexagon are all on equal distance from the sphere and will thus have to move the same distance. This leads to a regular hexagon in the middle of the triangle. Then from the centre point outwards circles can be found of points that are at equal distance from the surface. So although the mesh deforms a bit due to the projection to the sphere, there is still a high repeatability of the polygons. Then in the last step the edges of the polygons and the surface between the ribs of the polygons are set to match the sphere. This will lead to curved segments that follow the sphere perfectly. However, this does not influence the amount of different shapes in comparison to step 6, since the corner points of each polygon are already set. In figure 10 an example of the different shapes of the polygons in one triangular section of the icosahedron is given. The amount of different polygons is dependent on the dimensions of the triangle. For the example in the figure the dimensions are 2 hexagons as a radius and this leads to 4 different segments. But if, for example, the radius of 1 hexagon was chosen, 2 different segments would have come out, as can be seen in figure 10b.

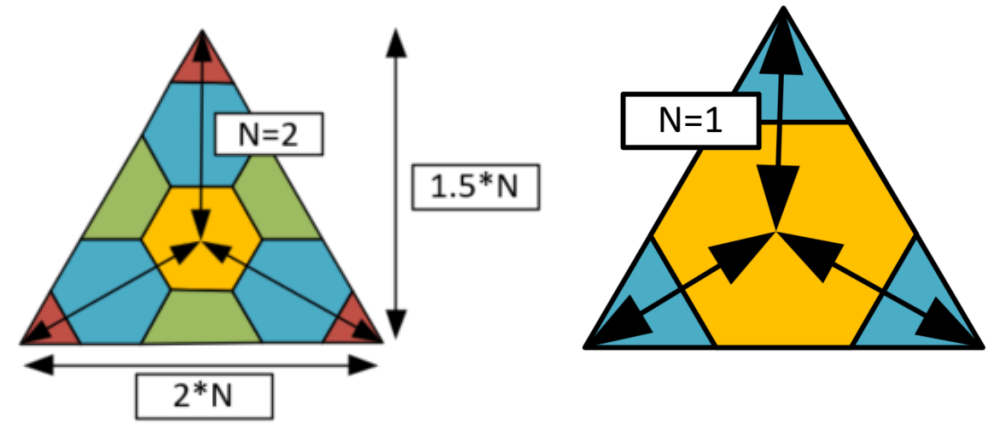

Figure 10: Visualisation of the different segments for diminsions N=2 (a) and N=1 (b).

To get the results described above, multiple Grasshopper plug-ins have been used next to the standard Grasshopper elements. The plug-in Parakeet has been used for creation of the icosahedron, Anemone to loop through the data sets, and Karamba 3D for identifying duplicate points and lines.

4.2 Structural analysis conditions

The Goldberg method as described above, helps to create a repeatable pattern on the surface of a dome. The size and the amount of different segments depends on the amount of hexagons that are fitted inside the triangle from step 3. In the literature review the maximum size of a module was discussed. The upper boundary is determined by the transport possibility and was set to a maximum of 2m in width. The situation that corresponds to this size limitation is the situation of N=4, following the principle described in figure 10. For the lower boundary there are no limits in terms of transport, but the smaller the segments are, the more segments need to be assembled. And thus increasing the workload. To compare the different sizes, situations from N=4 till N=10 are used.

To evaluate the influence of the different segment sizes a dome structure is used. For this the segmented sphere coming from the Goldberg method is used. The dome was said to have a span of 17.31m and a sagitta of 5m. To get this dome only shell segments are selected with their centre of gravity above a level of 5m. This way only whole shell segments are used in the model and no difference can be introduced by half cut modules. Because of the whole shell segments that are used, the base line of the dome is no longer on one level. The supports will be placed at the corners of the shell segments that lie on the base line. This is displayed in figure 11. The supports are created with the support element of Karamba3D, where the degrees of freedom are fixed in x, y, and z direction, but are free to rotate. In figure 11, the supports are displayed in green.

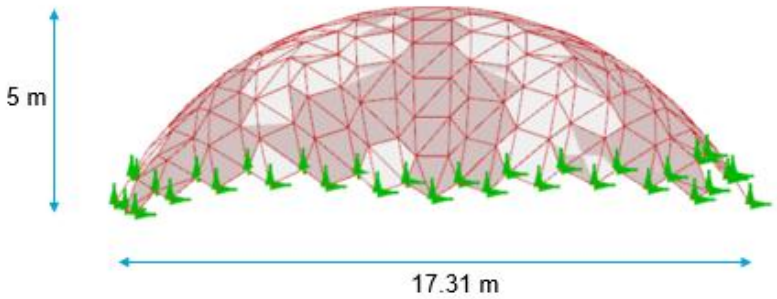

Figure 11: Dome structure with support locations.

The shell segments are created by putting the shell surface elements found in the Goldberg method in a Mesh Brep element. This Karamba3D element puts a mesh on each shell surface. This mesh is defined by a mesh resolution and an Edge refinement factor. The mesh resolution determines the

overall size of the mesh and thus the amount of elements that each shell module surface consist of. In the figure above a mesh resolution of 1.0 is used and it can be seen that the amount of segments in each shell module is relatively low. When the mesh resolution factor is lowered, the amount of elements in the model increase.
The edge refinement factor makes the mesh more concentrated around corners. This leads to smaller mesh elements around the corners and bigger mesh elements in the middle of the shell segment. This feature is mostly useful for abrupt or sharp changes in the shell surface. Since the dome structure is very smooth, the edge refinement factor will be kept at 1.0. (Harish, 2024)

The size of the mesh determines the accuracy of the model. For each mesh segment the results are calculated for displacement, and stress distributions. When the mesh segments are large, less calculations have to be made, and the model will be faster. But large mesh elements often also mean a less accurate result compared with the real situation. Therefore a smaller mesh might lead to a more accurate result, while increasing the computational time. There is a limit to how much smaller the mesh can be made. After a certain point, the computational time increases rapidly, while the accuracy of the model does not change that much anymore. The search for the optimal combination of computational time and model accuracy is called mesh convergence. [Harish, 2024]
For this purpose the mesh resolution factor will range from 0.1 till 1.0 for situations N=4 till N=10. To find the optimal resolution, the maximal deflection of the dome will be compared, as well as the potential energy in the structure, and the buckling factors.

The connections between the elements are simulated using the line joint element from Karamba3D. The rotational stiffness was estimated to be 104 kNm/m/rad. The line joints are put between every two adjacent shell segments. This can be seen in figure 12.

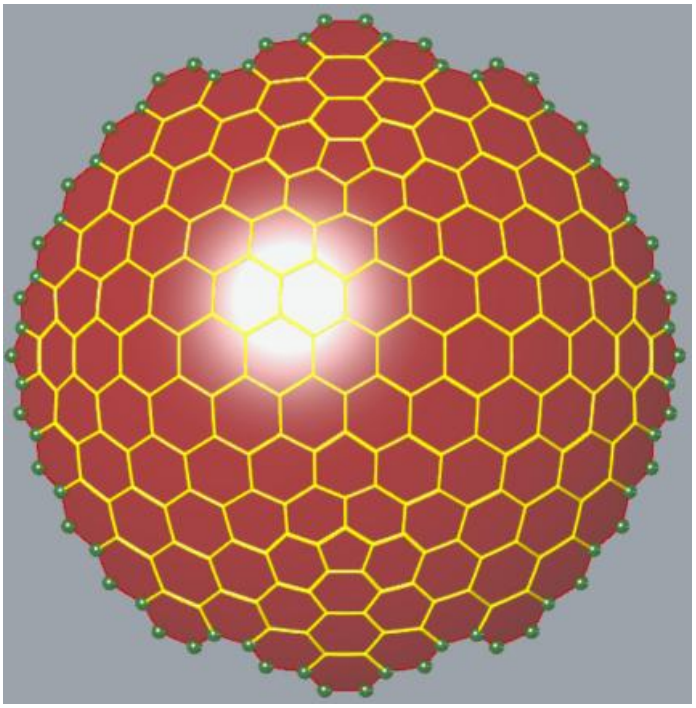

Figure 12: Dome structure with line joints between the elements. Here the line joints are displayed in yellow, and the supports in green.

All different elements are finally put together with the assemble model component and the system is calculated with the analysis-II component. This component performs a second-order analysis, which considers the influence of deformations on the structural stiffness. The analysis-I component can be used for a first-order analysis, but then it would be assumed that the deformations are small and

have a negligible impact on the overall behaviour of the structure. (Karamba3D, 2024) In shell structures the stability or buckling of the structure is governing over the forces in the structure. Therefore the analysis-II component is chosen over analysis-I to get a more accurate result in terms of stability.

When the different shell segment sizes are compared, one can be selected as the most optimal size. The results were based on shell segments that retained their shape in such a way that the base of the dome does not form a perfect circle. In reality the shell segments would need to connect an underlaying structure or foundation. On top of that the unregular base line acts a little bit like a clamp, since the shell is prevented from rotating by the supports on different heights. When the boundary lies on one line, the shell will have more rotational freedom and that should come closer to the hand calculation.
To provide a consistent flat boundary, two solutions will be investigated. The first is by sampling cutting the shell segments, where they exceed the boundary line. This method will allow the use of the original modules, which will make it easier and faster to construct the dome. However by cutting the shell segments, some amount of waste is produced depending on how much of the segment is cut away. The supports can then be placed on the cut module corners that lie on the boundary line. Solution two is to produce the sections on site with the original amount of formwork. This will create a continuous ring to which the shell modules can then be attached. This way the support condition can be changed to a more continuous support instead of supporting the shell only in the corner points.

In dome structures the forces accumulate in the apex of the dome. This makes it a critical point for the dome design. In construction the apex of the dome is also more difficult to reach. Because of difficult access, difficulties in compacting concrete, and uneven curing can occur. This makes it hard to ensure consistent material quality at the apex. Cracking or weaknesses can significantly compromise the entire structure. A commonly used solution is removing this area, by introducing an oculus. The oculus allows for redirection of the forces via a compression ring. This both simplifies construction and improves reliability. However, with modular construction the segments are already constructed using pre-fabrication. This removes the issue of the quality control, but difficulty of accessibility remains.
Other reasons for introducing an oculus lie in design considerations. An oculus can provide a gateway for natural light in a structure as well as ventilation. It can also be added as a aesthetic feature. In any case the influence of modular construction should be investigated to ensure the possibility of such a feature. The way this will be done is by cutting the modules near the apex, such that a perfect circle is created. The size of the oculus can be any size, as long as the dome remains stable. (Davis et al, 2016) For the stability a smaller oculus provides a better re-distribution of forces inside the shell. With a smaller oculus the forces have to re-distribute less, since there is more material left to take up the forces. Some of the reference structures from table 1 also have an oculus. In table 4 below the size of the oculus compared to the size of the dome is displayed.

Table 4: Dome-Oculus ratio.

Dome	**Dome diameter [m]**	**Oculus diameter [m]**	**Ratio [%]**
Pantheon	43.3	8.3	19
St. peter's Basilica	42	6	14
Taj Mahal	18	1	5

For the size of the oculus the average ratio of the reference structures is taken, which is about 12%. With the dome diameter of 17.81m, this leads to an oculus diameter of:

$$0.12 * 17.81 = 2.137 \sim 2m$$

A hole can also be introduced in another part of the structure, such as at the base to serve as an entrance. However, such a hole will disrupt the hoop forces at the base of the dome, where they are highest. This will significantly weaken the structure and because of this extra stiffening or different support conditions might be required. If this is done, those aspects might take away focus from the behaviour of the segmented shell, while the oculus should be able to be introduced without any other elements.
So the diameter of the oculus is taken as 2m, and is visualized in figure 13.

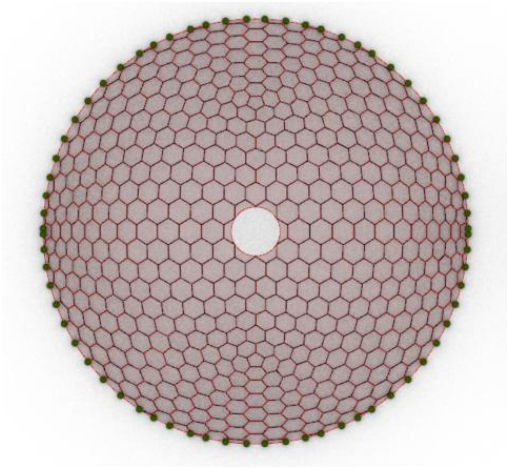

Figure 13: Dome with oculus.

4.3 Structural analysis

In this section the results of the mesh convergence, different boundary conditions, and of the structure with oculus will be displayed. The structure is modelled as described in section 4.2.

Mesh convergence

For the mesh convergence a structural analysis is done for the situations N=4, till N=10. For this the mesh resolution ranges from 1.0 till 0.1. Based on these parameters the elastic energy, maximal displacement, and the buckling factor are calculated for the two load cases. The results are plotted in figure 14 as a function of the amount of elements used in the analysis.

	Uniform load	**Wind load**
Energy	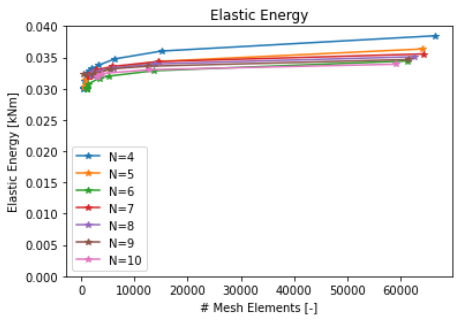	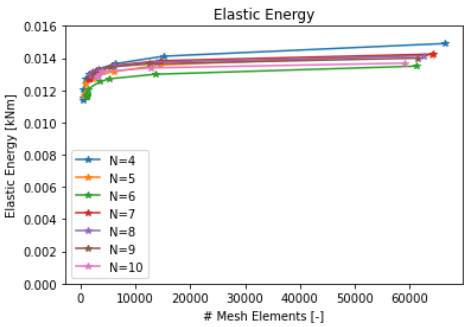

Displacement

Buckling

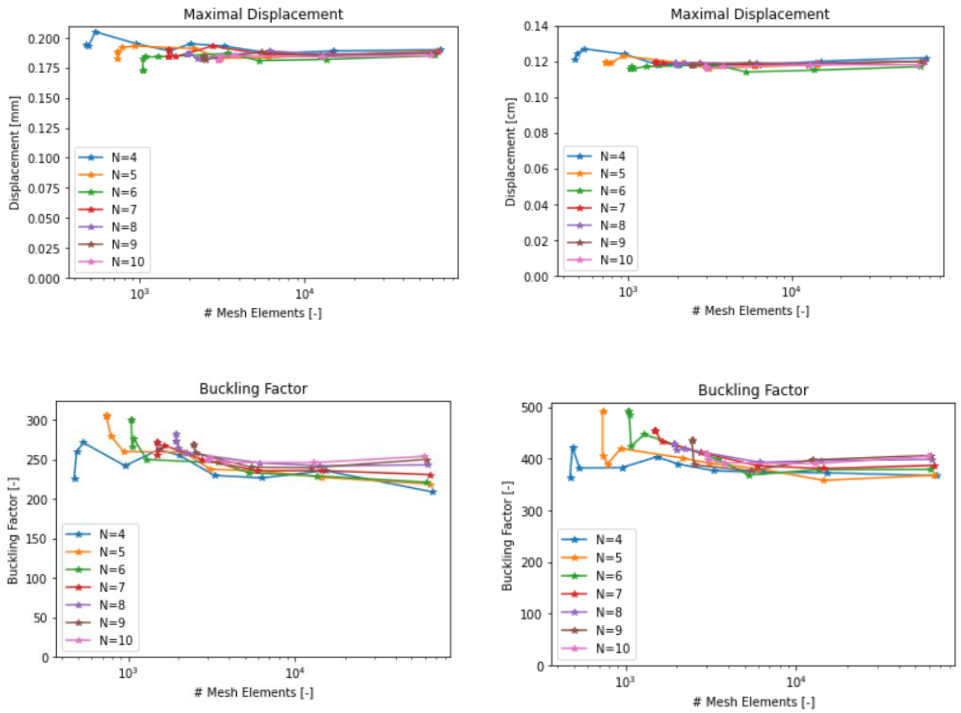

Figure 14: Results of the mesh convergence for the elastic energy, maximum displacement, and the buckling factor under the two load cases.

Starting with the figures for the elastic energy, it can be seen that the energy is slightly lower for a small amount of mesh elements. Then as the mesh elements increase, so does the elastic energy. When the amount of elements is starting to get large in number, the difference in elastic energy is becoming much smaller. Around 5000 elements, the graphs are almost flat for most of the situations for N. It can also be seen that for the lower values of situation N the elastic energy is higher than for higher values of N.

The graph for the maximum displacements is relatively flat. However, for a smaller amount of mesh elements there is more turbulence around the standard values of approximately 0.19 mm, and 0.12 mm for the uniform load, and the wind load respectively. For lower values of N, there is slightly more turbulence for smaller amount of mesh elements. In the figure a logarithmic scale has been used in order to better differentiate the turbulence in the results. In the figures for the elastic energy can be seen that the values for lower number of mesh elements lie very close together. Although this works to visualize the convergence of the model in the elastic energy, this becomes unclear for the displacement. After approximately 5000 mesh elements, the graphs for the displacement become stable for every value of N.

The last two graphs depict the buckling factor for each situation. Just as with the displacement a logarithmic scale has been used to be able to more clearly tell different results apart for smaller amounts of mesh elements. A similar pattern can be seen as was found for the displacement. For a small amount of mesh elements there is more turbulence in the results, while a larger amount of mesh elements results in a more stable outcome. The stabilisation of the graphs again happens around 5000 mesh elements. Once the graphs are stable it can be observed that the situations with a higher value of N give a higher buckling factor. It can also be noted that the values for the buckling factor are very high. So the cross section found with formula 2 was an overestimation for the created dome structure. However this research focuses on structural behaviour of the segmented shell and for that the thickness of the cross section does not need to be reduced.

From the above results, it can be concluded that the model converges around 5000 elements or a mesh resolution of 0.3. With more elements the results still change slightly, but this difference is

small. The amount of mesh elements increase rapidly with the decrease of the mesh resolution factor and therefore take more computational time. From the different situations of N can also be concluded that larger shell segments give on average more turbulence in the results for the displacement and buckling factor, while the smaller segments are more stable. The elastic energy for larger segments is also higher than for smaller segments. This indicates that the force distribution inside the structure happens more efficiently for smaller shell segments. Situation N=8 is taken as the situation to continue with. This situation gives a good result in terms of elastic energy in the structure, while the computational time is still reasonable.

Boundary conditions

For the influence of the boundary conditions on the structural behaviour situation N=8 is taken as described above. Four different situations are to be considered, of which the first uses the boundary conditions used in the mesh convergence. The second uses the same boundary conditions, but the stiffness off the joints is set to infinitely stiff to simulate a continuous shell structure. For the third situation the shell segments are cut at the base line, and for the last situation a continuous ring is constructed replacing the segments that were cut in the third situation. The results of the deflection, and principle stresses are displayed in figure 16 and 17. In the results sigma 1 represents the meridional stress going from the base of the dome to the top. Sigma 2 corresponds to the hoop stress and acts perpendicular to sigma 1 in a horizontal direction. For the structure under wind load, the orientation of the forces changes slightly. The point where the forces are directed to shifts a bit, and sigma 1 is pointed to this new point. Sigma 2 still follows a circular pattern perpendicular to sigma 1. The compressional forces in the structure will be denoted with a negative value, while tensional stresses will be denoted by positive values. The colour range can be found in the figures.

The elastic energy, maximal displacement, and buckling factors of the structures are shown in table 4 and 5.

1

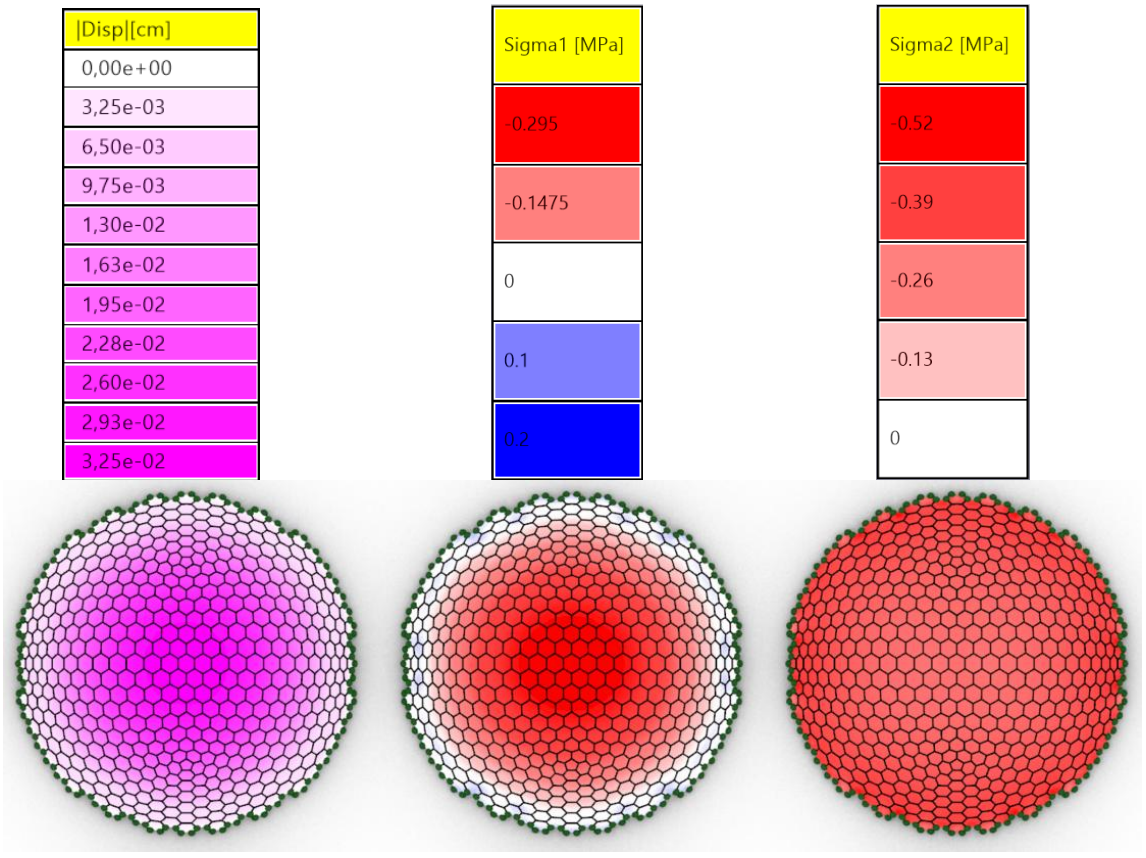

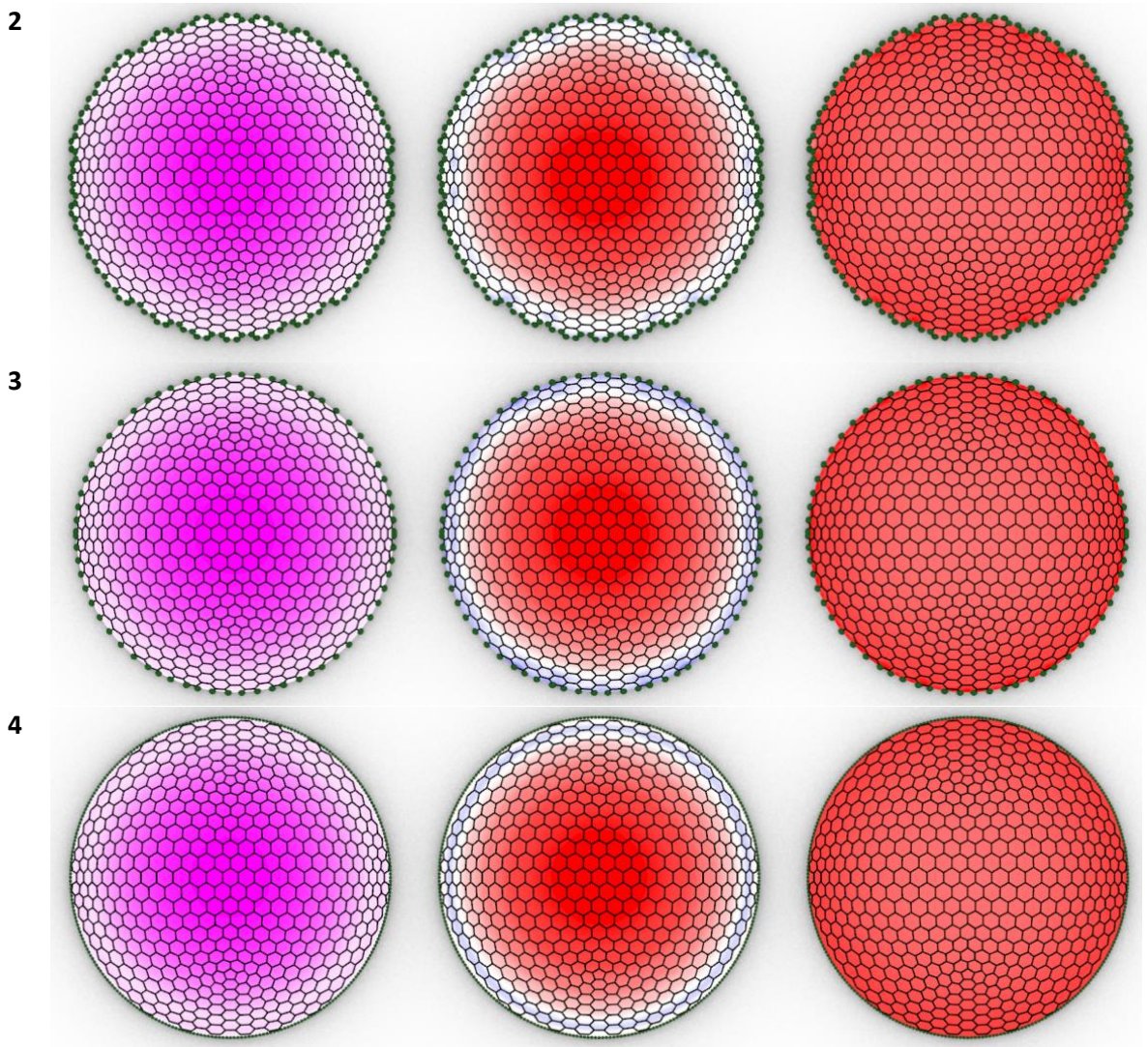

Figure 15: Displacement field, and principle stresses in the dome for the different boundary conditions under uniform load. BC 1 (Boundary Condition) has whole modules, BC2 has stiff joints, BC3 has cut modules at the boundary, and BC 4 has a continuous boundary

Table 5: Characteristic values for the dome in the four different situations under uniform load.

Situation	**1**	**2**	**3**	**4**
Displacement	0.019 cm	0.019	0.019	0.019
Energy	0.034 kNm	0.034	0.037	0.033
Buckling factor	241.9	266.5	250.1	248.3

In figure 15 and table 5 can be seen that the displacement field and the stress distribution does not change much between the different situations over the entire structure. At the boundaries it can be seen that the uneven boundary line of situation 1 and 2 results in a more uneven stress distribution where there are patches of tensile stresses along the boundary. In situation 3 these patches also occur, but the difference is that the tensile stress is more uniform and slightly higher in force than it was for situation 1 and 2. Lastly in situation 4 the tensile ring is much more smooth and does no longer contain outliers. Another thing to notice in this situation is that at the boundary the stress is near 0 while in situation 3, the tensile stresses also occurred at the boundary itself. In all situations the amplitude of these stresses remain well within the boundaries of the material properties of C20/25 as can be seen in the legends of figure 15.

In table 5 can be seen that all situations give the same displacement in the dome. The energy however is slightly different for the different boundary conditions. Situation 4 gives the lowest value, while situation 3 gives the highest value. Although the values are slightly different, they are still very close to each other. The buckling factor displays the biggest difference. Situations 3 and 4 give about the same result, while the uneven boundary of situation 1 gives a slightly lower value for the buckling factor. This changes again however in situation 2. Here the same boundary conditions are applied as in situation 1, but the joints are set to infinitely stiff. With the stiff joints the buckling factor is highest out of all situations.
In figure 16 the results for the wind load are given and it can be seen that the stress is distributed more equally than it was for the uniform load. The patches of high stress that were observed in the uniform load condition are not seen in the wind load condition. However there are still some small fluctuations at the different boundary conditions. In all situations higher tensile stresses are reached for sigma 1 over a larger area. In table 6 can be seen that the value for the buckling factors is much higher than for the uniform load situation. With the relative low forces in the structure compared to the material qualities, the buckling load factor drives the design.

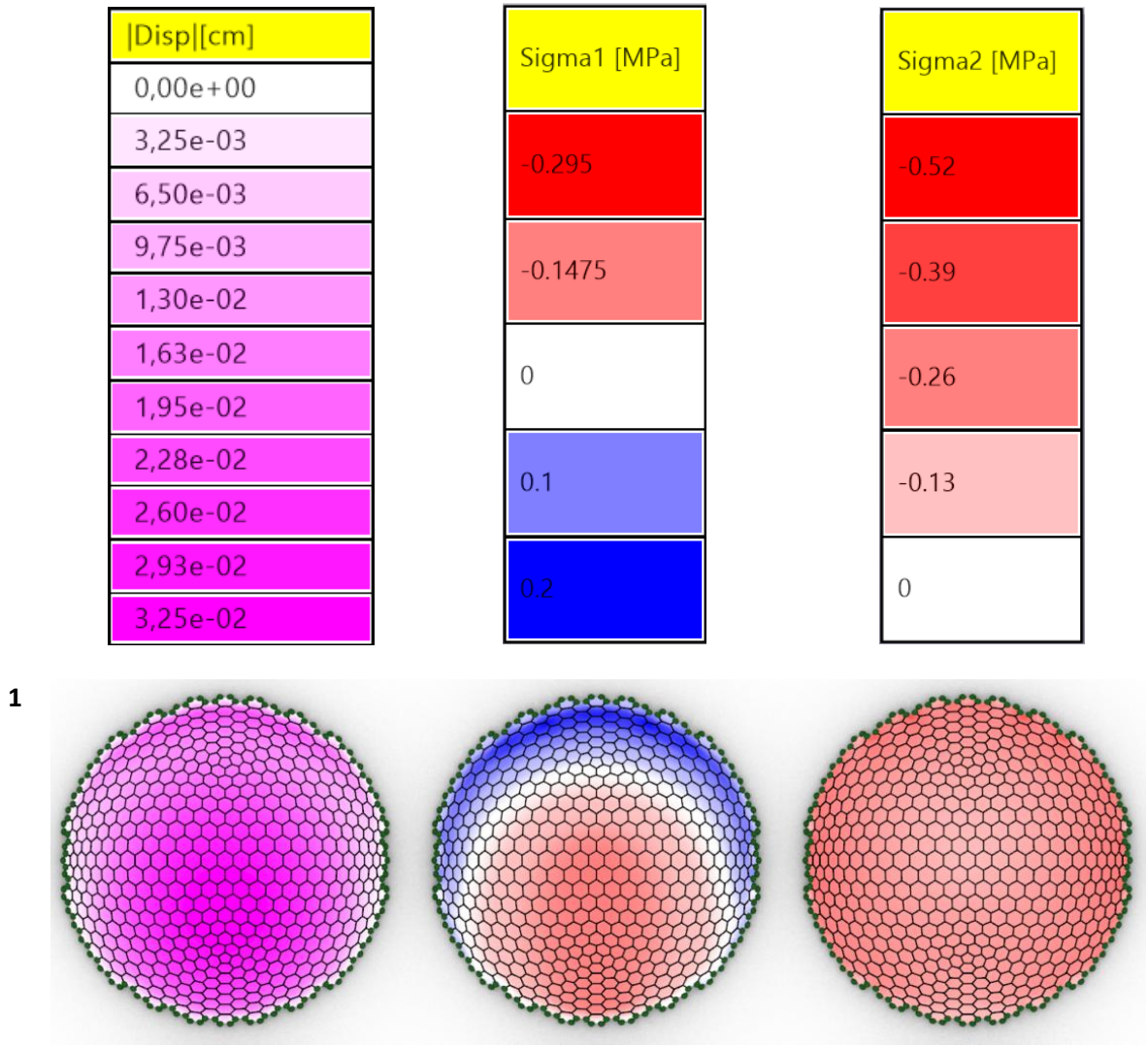

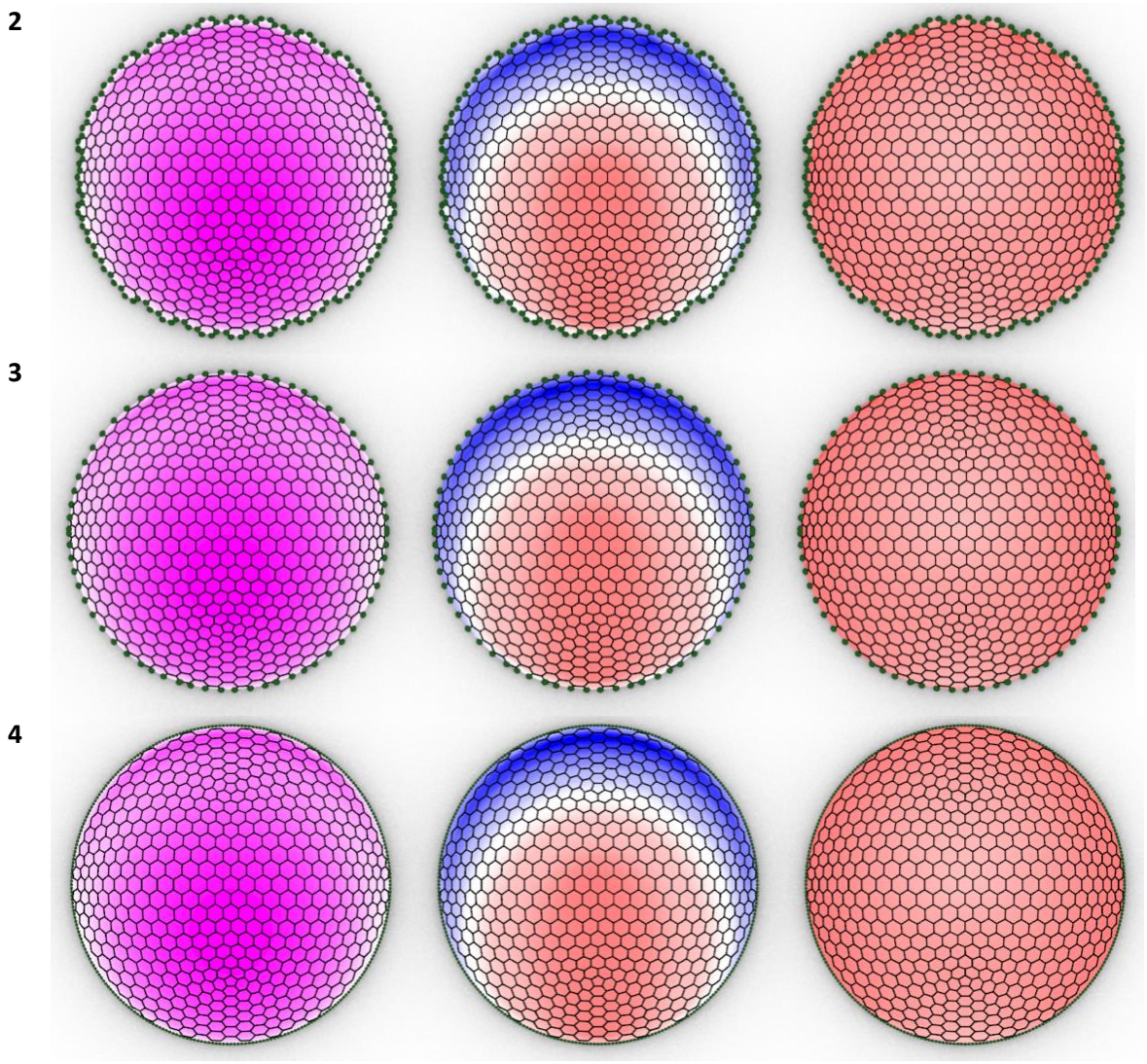

Figure 16: Displacement field, and principle stresses in the dome for the different boundary conditions under wind load. BC 1 (Boundary Condition) has whole modules, BC2 has stiff joints, BC3 has cut modules at the boundary, and BC 4 has a continuous boundary ring. Supports are shown in green.

Table 6: Characteristic values for the dome in the four different situations under wind load:

Situation	**1**	**2**	**3**	**4**
Displacement	0.012 cm	0.012	0.012	0.012
Energy	0.014 kNm	0.014	0.015	0.014
Buckling factor	396.6	426.0	408.4	400.8

Dome opening

In figure 17 and 18, the influence of an oculus in the structure is investigated as was discussed in section 4.2. The same boundary conditions will be used as in figure 15 and 16, leading to a new force distribution, displacement field, and stiffness. The results can be found below.

|Disp|[cm]
0,00e+00
3,40e-03
6,79e-03
1,02e-02
1,36e-02
1,70e-02
2,04e-02
2,38e-02
2,72e-02
3,06e-02
3,40e-02

Sigma1 [MPa]
-0.5
-0.25
0
0.18
0.36

Sigma2 [MPa]
-1.02
-0.765
-0.51
-0.255
0

1

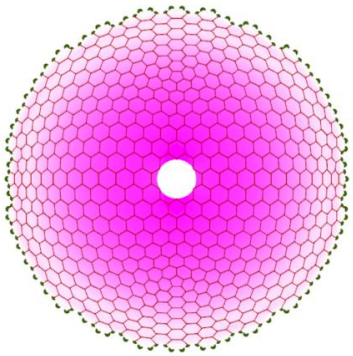

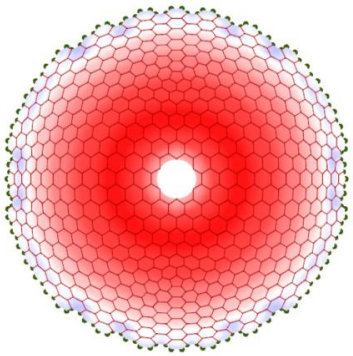

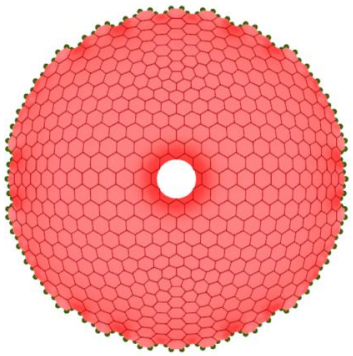

2

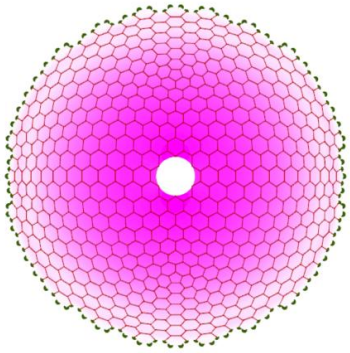

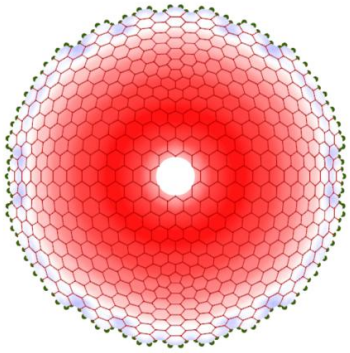

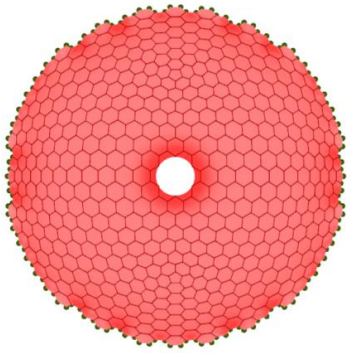

3

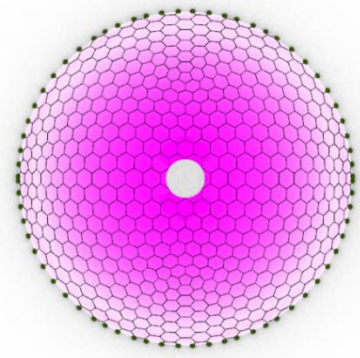

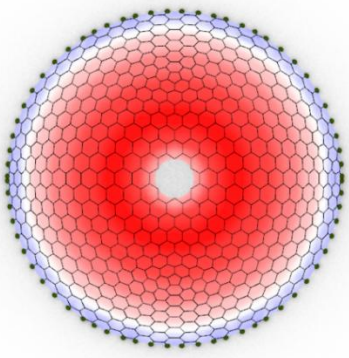

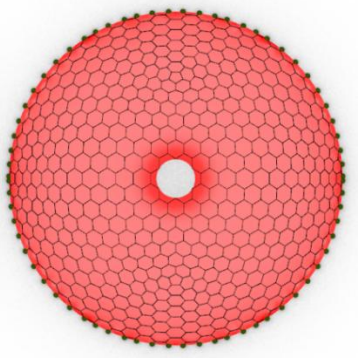

4

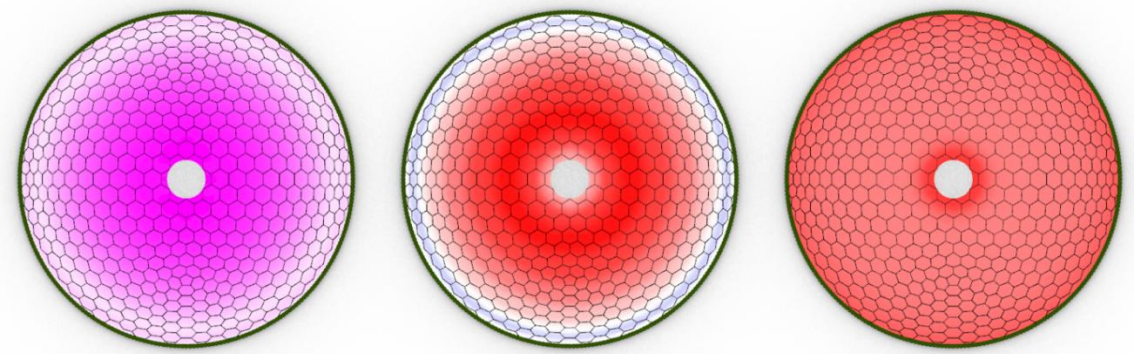

Figure 17: Displacement field, and stress distributions for the situations with an oculus under uniform load. Supports are shown in green.

Table 7: Characteristic values for the dome in the four different situations with oculus under uniform load:

Situation	**1**	**2**	**3**	**4**
Displacement	0.034	0.033	0.033	0.031
Energy	0.055	0.055	0.061	0.054
Buckling factor	21.9	27.2	21.6	21.8

In figure 17 can be seen that the oculus takes away the critical point at the apex. And the forces are redirected around the oculus forming a compression ring. However, compared to the structures without oculus, the stresses became slightly higher. The stresses are still well within the boundaries of the material. In table 7 can be seen that, even though the elastic energy of situation 3 is still a bit higher than the other situations, all values are now closer together than without the oculus. The stiff joints of situation 2 do still have influence on the stiffness of the structure. In figure 18 the behaviour of the structures under the wind load are given. Here the same observations can be made as for the uniform load.

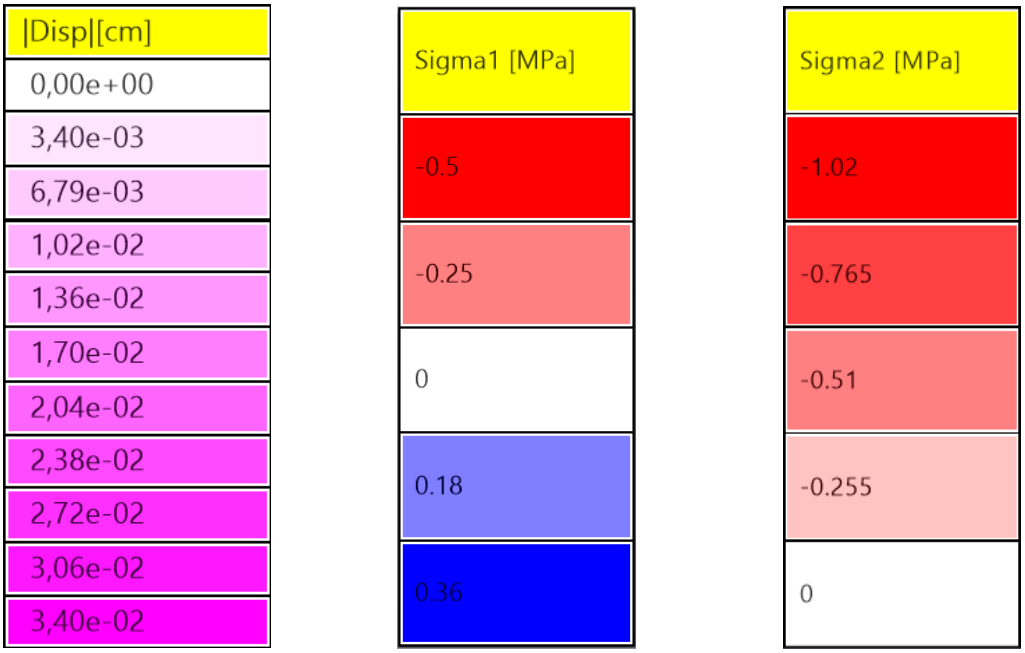

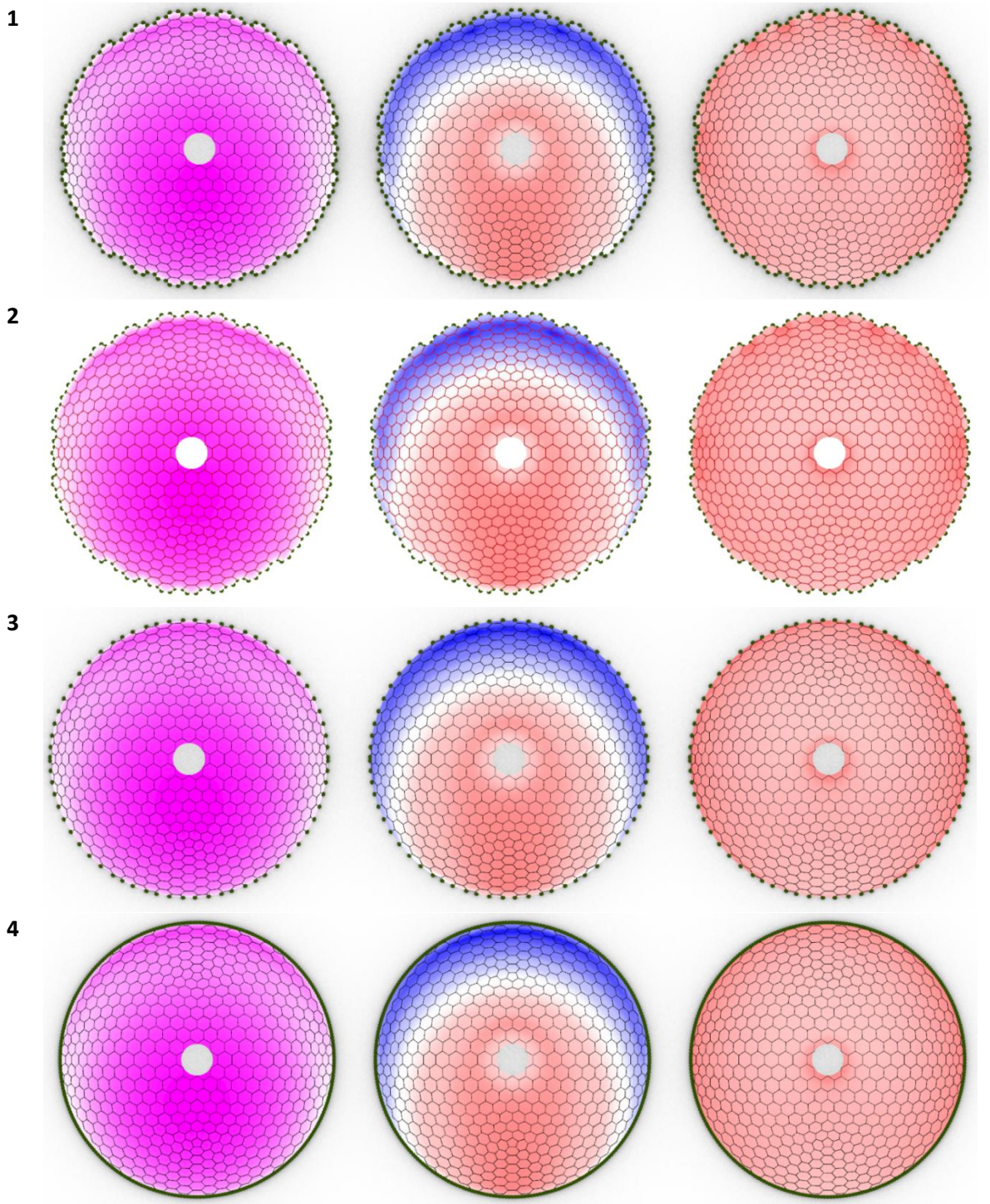

Figure 18:Displacement field, and stress distributions for the situations with an oculus under wind load. Supports are shown in green.

Table 8: Characteristic values for the dome in the four different situations with oculus under wind load.

Situation	**1**	**2**	**3**	**4**
Displacement	0.021	0.020	0.021	0.020
Energy	0.022	0.022	0.025	0.023
Buckling factor	43.8	54.4	43.2	43.7

The now comparable buckling factor between situation 1, 3 and 4 indicate that the boundary conditions no longer have influence on the buckling stiffness of the structure. Instead the oculus introduces a new critical point that buckles outside the influence of the boundary conditions. To validate this the buckling mode of situation 4 under the uniform load, with and without oculus are shown in figure 19. Without the oculus the structure buckles globally in circular patterns, but with the oculus the buckling mode changes to local buckling around the oculus.

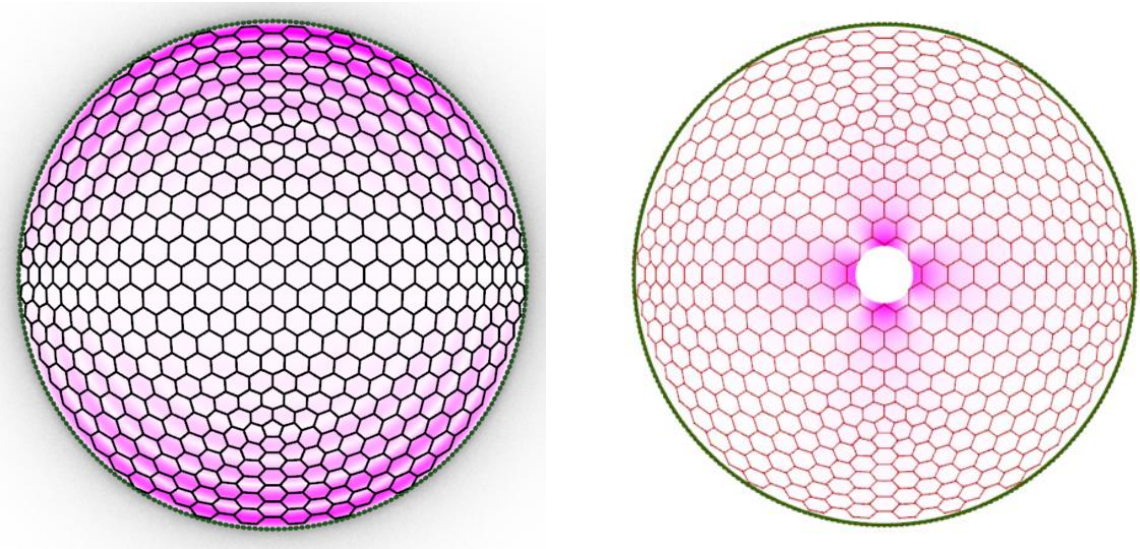

Figure 19: Buckling mode for the structure without oculus (left) and with oculus (right). Supports are shown in green.

5. Clustering

This chapter will discuss the steps that were taken to subtract a set of modules from the pattern created with the Goldberg method as well as the results this leads to. Then the modules are further optimized, using k-means clustering for the edges of the modules.

5.1 Finding modules

To find the different modules there will be looked at the way the shell segments in the dome were created. In the Goldberg method an icosahedron was used to represent a sphere and the hexagonal mesh on the icosahedron was then projected onto the sphere. The amount of distortion of every hexagon depends on the distance to the sphere. The corners of the icosahedron are located on the sphere and from there to the middle of each face of the icosahedron the hexagons get more and more distorted. So the shell segments can be clustered based on their distance to the corner points of the icosahedron. In figure 20a this principle is displayed, where each unique distance to one of the corner points gets a new colour. This leads to 18 different modules. However, the hexagons that are cut in half along the edges of the triangle, will have a different shape than a full hexagon on the same distance. If we assume that the formwork can be made in such a way that mirrored hexagons can be produced without problem, 2 more modules should be added to account for the half hexagons that share a circle with whole hexagons. In figure 20b the resulting pattern of modules on the dome structure can be seen.

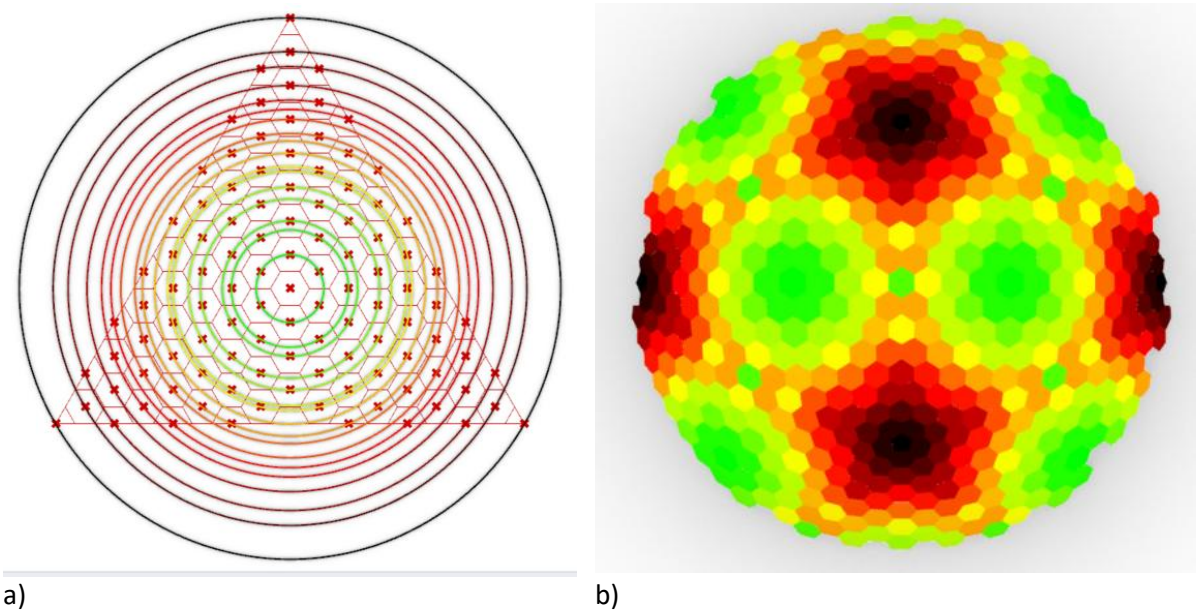

a) b)

Figure 20: a) Visualization of different distances from the middle. b) Different shell segments in the dome structure.

In figure 21 below all the different modules are lined up with their dimensions displayed.

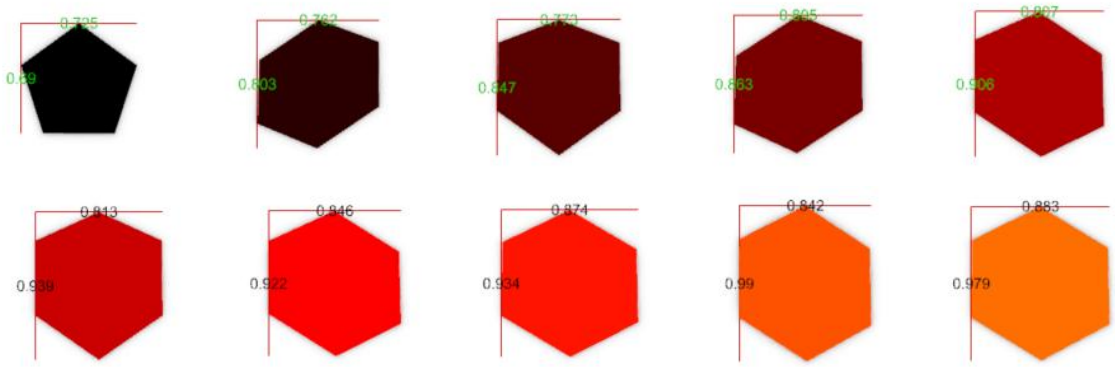

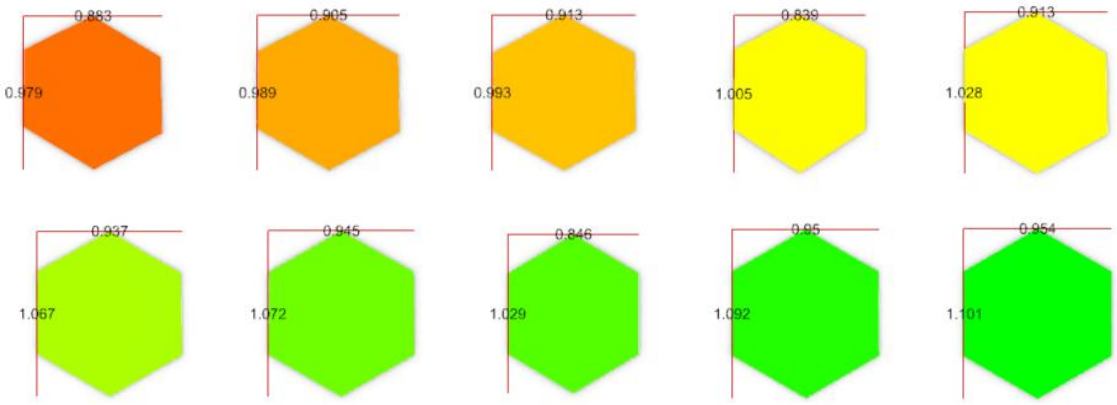

Figure 21: Set of modules obtained from the Goldberg method.

5.2 Module optimisation

The modules from figure 21 are exactly fitting for the dome structure used in the structural analysis. However it would be more optimal if the modules are able to describe a variety of structures and not only the dome they were based on. For this purpose the modules need to be further optimised. To optimise the possibility of different configurations the edges of the modules can be clustered based on their length.

The modules from figure 21 have 34 different edge lengths ranging from 398mm to 550mm. In NEN-EN 13670:2009 it is stated that the dimensions of the cross-section for beams, plates, and columns can have a deviation of $\pm 15\ mm$ for cross sections with a width around 400mm. (NEN-EN 13670, 2009) These construction margins are important to ensure manufacturability, structural integrity, and compatibility between components. Manufacturing machines can have an error in their production, so if the elements are assumed to connect perfectly a problem will arise in the assembly of the elements. Tight margins may improve fitting of the elements, but increase the manufacturing difficulty and with that the manufacturing becomes more expensive. More loose margins may reduce the cost, but then elements connect less accurately to each other. Therefore edges are clustered together if they have a maximum difference of 15mm, following NEN-EN 13670. Later, the influence of smaller margins will also be investigated.

In order to optimise the found modules and make them more suiting for reconfigurable patterns, the edges of the modules are adjusted in such a way that the amount of different edge lengths decreases. For this k-means clustering is used based on the edge lengths. From all different edge lengths, the two closest edge lengths are clustered and all edges in that cluster are replaced with the shorter version of the two. This will leave a small gap between the replaced edges and the adjacent edges. To resolve this, the adjacent edges are pulled towards the new edge corners. Now the modules have closed boundaries and the procedure can be repeated for these new slightly adjusted modules. This will go on till all edge clusters differ more than the allowed 15mm in length. This results in the module set in figure 22.

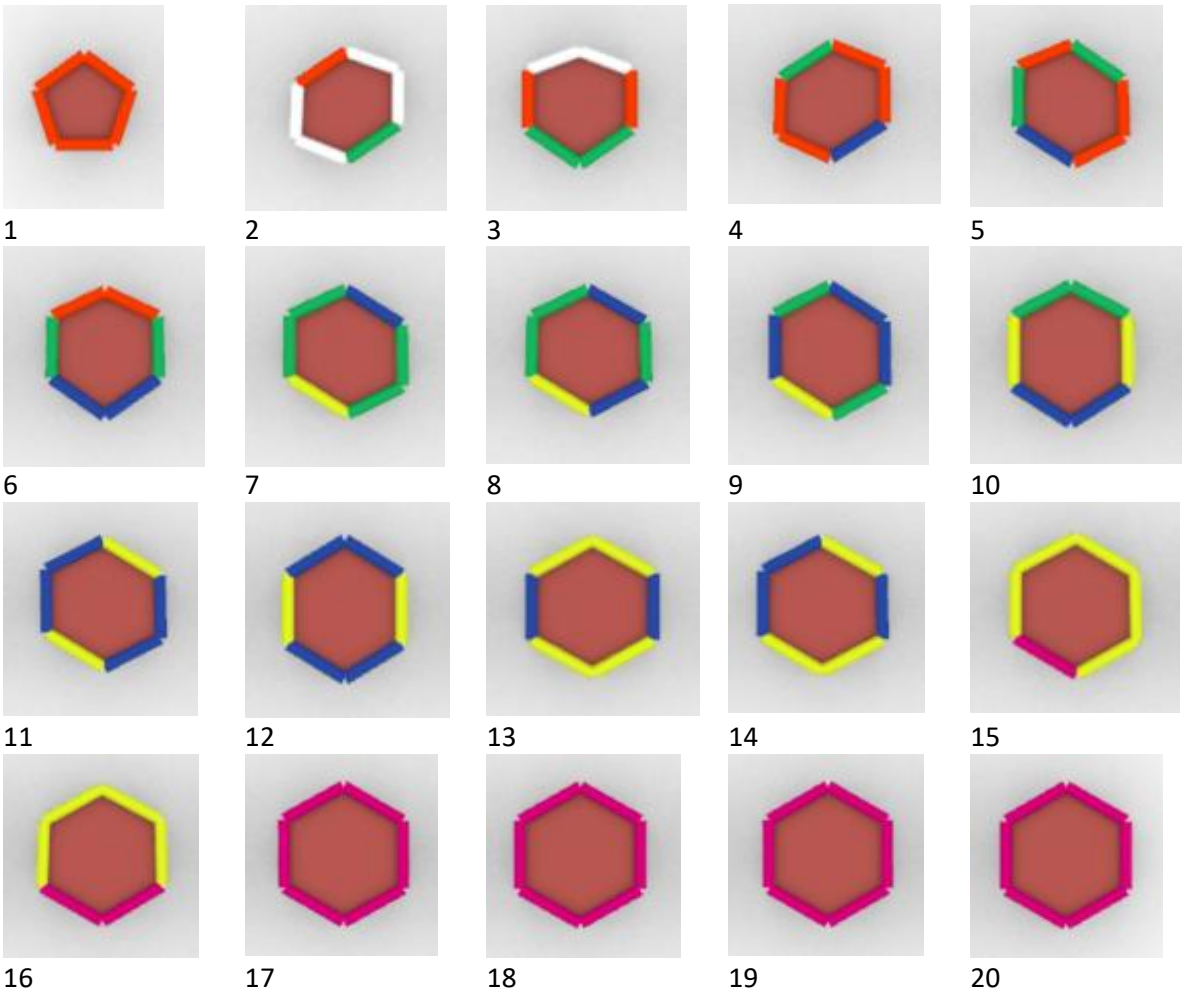

Figure 22: Set of modules after clustering.

With the clustering method as described above, the amount of different edge lengths has been reduced to 6 different values. In figure 22 can be seen that some modules look very similar to one another. The modules 17, 18, 19, and 20 all have the same edge length for every side. When the modules are placed on top of each other the differences can be measured by looking at the distance between the corner points of the module. The distance between the corner points of the modules shows that they are slightly different from each other. However, all corners lie within a range of 6mm to less than 1mm. So although slightly different they are very similar.
Module 11 and 12 are also very similar and comparing them leads to a corner distance between the modules of maximal 5mm and minimal 2mm.

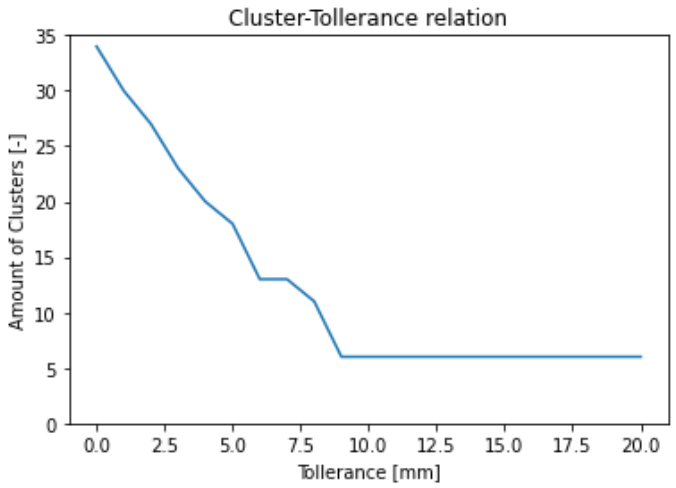

Figure 23: Relation between the amount of clusters made and the construction tolerance.

The modules from figure 22 are obtained with a tolerance of 15mm. In different situations the accuracy of the modules might be needed differently. In figure 23 the amount of clusters are plotted against the chosen tolerance. When the tolerance is set to 0 the original 34 different edges are found. With the increase of tolerance, the amount of different clusters gradually decreases until a tolerance of 9mm is reached. From there the amount of clusters remains on 6 different edges even exceeding the 15mm prescribed by NEN-EN 13670.

6. Discussion

This thesis delved into the use of modular construction in shell structures. Modular construction will help to reduce the environmental impact of shell structures. By finding a limited set of modules, the energy and material usage can be reduced in the way of prefabrication methods. It can also increase the reusability of formwork, and shell segments. Ideally a set of modules can be found that is able to describe a variety of different shell structures, allowing modular construction for shell structures to be used to the same extend as that for beams, columns, and slabs. This is an ambitious and complex goal and will not be reached by this thesis alone, but a first step in this direction is made.

6.1. Design considerations

In order to come to a set of modules, multiple methods have been used. Firstly it is attempted to obtain a set that can describe the largest possible amount of different structures. A radius of curvature of 10 meter was chosen for the design, using existing structures as a reference. In these reference structures was also seen that between and even within structures a variety of different curvatures are possible. By selecting one specific curvature, the design of any structure using the found set off modules will have to use this curvature. Assuming that different configurations are possible, a different curvature could also be achieved using the same set, since the curvature is also determined by the angle the modules are connected under. However, even if that is possible, the curvature will likely not differ that much. Therefore, each design using the shell modules will have to make a trade-off between mechanical efficiency, construction rationality, and circular reconfigurability

The design choice for a synclastic shape also means that the found modules can only be used for a shell structure that features a synclastic shape. The synclastic shape is a widely used shape in shell structures, since it is a shape needed to form most structures. However, this design leaves out anti-clastic, segments curved in one direction, and flat segments. Without modules to cover these type of curvatures, the found set can describe only a limited amount of structures. So even though the synclastic shape brings a very useful shape into the set of modules, it is not the only type of shape that is needed to complete a fully functional module set. So therefore the found set can be extended with different shapes.

To come to a module set the Goldberg method has been used to create a repeatable pattern on a spherical structure. For that a hexagon dominant mesh has been used and projected on an icosahedron. The icosahedron represents a spherical shape best out of all platonic solids, and with the use of only one type of polygon the same repeatable pattern can be used all over the sphere. This is an advantage over other shapes that represent a sphere, but on the other hand relatively few faces are used in the icosahedron compared to Archimedean solids. This leads to larger faces, with more polygons fitted into them, and more different distortions with the projection onto the sphere. With the Archimedean solids the faces are already smaller leading to more repetition on the surface and less shapes in the repeatable patterns, leading to a smaller selection of modules. However, with the Archimedean solids there is more than one type of polygon used in the solid. This will lead to the requirement of a creating a mesh in each different polygon. These meshes also need to connect to one another in order to create modules for the transition area. So even though the faces in an Archimedean solid are smaller, and thus should produce a lesser amount of modules, they also come in at least two different polygons. This will increase the amount of modules, and it will complicate the design. Because of this, the platonic solid was the more reliable option.

Assumptions

With the creation of the model some assumptions have been made for the supports and the line joints. For the supports it was assumed that each support was fixed in x, y, and z direction, and no resistance for rotation in any direction. In reality support connections can give some amount of resistance, even if it is a small amount. It is also possible that the boundary is not entirely restricted in horizontal direction, which allows the structure to deform a little at the boundary.

The line joints have been given an rotational stiffness. However this only works for rotation around the joint. Any deformation in other directions is made impossible, because of an infinitely stiff value. This might lead to a more stable and stiff structure. However the main orientation for joint rotation is taken into account and is expected to have the largest influence. Another assumption for the joints is that there is a perfect alignment between the different modules. Leading to an even joint width, and an evenly distributed force transition. In reality the alignment is not perfect and small deviations can occur during construction, possibly leading to peaks in the stress distribution. However, these types of deviations are covered with safety factors in the design.

With the finite element analysis the surface is approximated with flat mesh segments. The mesh segments along the edge of the modules need to connect to the line joints. However, if the original mesh is used as the input for the line joints, the model will run normally, but will give results that are slightly off. This is because the edges of the finite elements do not perfectly align with the original curved mesh. That small deviation will either cause the model to return wrong values, or it will make the model crash. Either way, it will not give an error message, making it difficult to spot.

6.2. Results

The results of the model come close in terms of stress in the top of the dome, but are slightly different for the stress at the base as well as the overall deflection.
It is because of the different assumptions for the boundary conditions. In the formulas the boundary condition was assumed to have some freedom to deform in horizontal direction. In the model all supports were fixed in place. This leads to a more strict boundary that the structure needs to conform to, leading to less deformation at the base and therefore also a smaller maximal deflection. The fixation of the points also leads to higher stresses at the base, because the structure is forced into a certain position. So although the model gave slightly different results from the formulas, the results are close enough to make believe that the model is correct. And at the top of the dome the stress does comply with the hand calculation. This is because the centre of the dome is not influenced by the boundary conditions as could be seen in the stress distributions.

Buckling is the governing difference between the segmented shell and the uniform shell. The buckling factors found with the assumed cross-section of the shell are very high for the closed domes. The cross-section can be a lot thinner in the given conditions, however the focus of this thesis lies in investigating the structural behaviour of segmented shells and finding a set of modules. For that the shell does not have to be optimised in terms of cross section.
The force distribution between the segmented shell and the continuous shell did not differ at all. Only the different boundary conditions gave slightly different results. Although the boundary conditions were different from each other, this research did not include large disruptions at the base such as an entrance. The oculus at the top of the dome did not influence the different boundary conditions and was the only option to include a hole without the need to add additional stiffening elements or change in supports.

Then for the clustering of the modules the circle pattern is a good way to separate them. The clustering of the edges worked well with the 15mm tolerance. With this tolerance it is in compliance with more commonly used tolerances. Larger tolerances also lead to the same amount of different edge lengths. And although a gap can help with covering up misalignments, it also introduces a larger weak point, because, as was found in the structural analysis, the segmentation of the shell leads to a lower stability. The bigger the gap, the larger the transition area between the shell segments and the more rotation is possible between the segments. This will most likely lead to a less stiff structure. Also with bigger gaps, the risk of cracking in the mortar will increase.
With more mortar there is more space for realignment though. And that will help with finding different configurations. For the different configurations it will help that the amount of different edges were reduced to 6 edges. This way a lot more combinations can be made, although it must be kept in mind that even though the edges are fitting, the inner angles of each connecting modules

need to comply as well. Depending on those angles perhaps even slight variations in the overall shell curvature can be made. With the grout gap there is also some room for deviation from the perfect alignment. On its turn this may then lead to an uneven width of the grout line. Another study would be needed to see what the limitations of this are.
As mentioned before as well, the found set of modules is only useful for purely synclastic shapes. For more complicated structures, it can still be useful, but as a part of a larger set. The larger set will need anticlastic modules and transfer modules to be complete. And the modules found in this study can also be tested in a topology study to see how useful they are in different configurations.

So it was found that the main influence of segmentation is the stability of the structure in terms of buckling load factor. In terms of force distribution the segmentation is not of influence. The smaller the segments and the higher the number for N, the more efficient the structure becomes with a lower elastic energy. Keeping in mind the constructability as well as the computational time of the model, situation N=8 is taken as the most optimal module size. This situation gives a good elastic energy, which is not that much higher from N=9, and N=10. Also the size of the modules is a little larger in those situations, meaning that there are less modules needed in a structure. This will reduce the workability of the structure, since there will be less elements to connect, compared to higher values of N. The model gives a near converged solution around 5000 mesh elements.

From the situation N=8 a set of 20 different modules was found. With the use of k-means clustering for the module edges, this amount can be reduced to 16 modules, with only 6 different edge lengths. This clustered solution is more suitable for different configurations. Although a topology study is needed to see how useful the set of modules really is.

7. Conclusions and recommendations

This research investigated how modular construction can be applied on shell structures. This construction method will help to improve the sustainability of shell structures. Modular construction is already being applied for standard building elements, such as columns, beams, and plates. The application stays behind for shell structures, where the complex structural shape leads to complex, and often one time use of formwork. This leads to waste production and a limited potential for reusability. Leading to the research question: How can modular design be used in shell structures?

The first aspect was to find a suitable geometry for the module design. A hexagonal dominant pattern was selected because of the limited amount of connecting modules in one corner, making alignment of the modules more easy, and because of the high amount of edges compared to other polygons that can be used for different configurations. A radius of curvature of 10m was selected as the most optimal curvature for a synclastic shaped set of modules. With the Goldberg method a modular, repeatable pattern has successfully been created.

With a structural analysis it was found that smaller modules give a more efficient structure in terms of buckling stability and force distribution. While larger segments results in less different shell segments and reduce construction time. A balance between structural efficiency and constructability was found for situation N=8. For this situation the influence of segmentation, as well as the use of different boundary conditions has been investigated. Leading to the finding that modular construction reduces the buckling stiffness, but not in such amount that modular construction would not be possible. The structural analysis showed that modular shell structures can provide sufficient strength and stiffness under different boundary conditions, and openings in the structure in the form of an oculus.

From the found optimal situation N=8, a set of 20 modules have been extracted. With the use of k-means clustering these modules were further optimised, leading to a reduction to 16 different modules with only 6 different edge lengths. This increases the usability in different configurations.

Below the main findings of this thesis are listed:

- Modular construction is very possible within shell structures.
- Segmentation reduces the buckling stability of a structure.
- An optimal module size was found between 0.7mx0.7m and 1.1mx1.1m for situation N=8.
- A set of 16 different modules can be created with 6 different edge sizes.

7.1 Limitations

The results are positive for the usage of modular construction of shell structures. However, the models used in this thesis also have some limitations. One of these is that the model assumes perfect alignment between the shell segments, not taking into account the small adjustments in module shape coming from the k-means clustering.
Also the found modules have not been tested in a topology study and therefore it is not yet known how many configurations they can make.
The usability of the module set will also be limited due to the synclastic shape of all modules. To be used in a wider context, anti-clastic modules, modules curved in a single direction, and potential transition modules should be added to the set.

7.2 Future work

To address the limitations of this research and to extend the findings of this research, multiple topics can be investigated.

A topology study using the found module set can be performed. By doing so, the extend of the usability of the module set can be investigated. Seeing how many configurations can be made and what variety of curvatures can be described with them, can quantify the value of the module set. The topology study can be followed by a structural performance test, using the modules in their different configurations. Both topics will have to take into account the possible misalignments that fall within construction margins.

Another study can continue this thesis by looking into more complexly shaped structures including anti-clastic curvature. For this the structural behaviour can be investigated, as well as finding new modules to extend the module set. By doing so the usability of the shell modules will increase.

Bibliography

85/3/EEC. (1985). *319885L0003*. Retrieved from eur-lex.europa.eu: https://eur-lex.europa.eu/legal-content/EN/TXT/HTML/?uri=CELEX:31985L0003

ArcGIS. (2024). *Why hexagons?* Retrieved from pro.arcgis.com: https://pro.arcgis.com/en/pro-app/latest/tool-reference/spatial-statistics/h-whyhexagons.htm

ArchDaily. (2013, November). *Heydar Aliyev Center / Zaha Hadid Architects*. Retrieved from archdaily.com: https://www.archdaily.com/448774/heydar-aliyev-center-zaha-hadid-architects

Archdaily. (2024). *www.archdaily.cl*. Retrieved from Archdaily: https://www.archdaily.cl/cl/949213/pabellon-portalen-map13-barcelona-plus-summum-engineering-plus-edyta-augustynowicz/5f7e012a63c017723f000358-portalen-pavilion-map13-barcelona-plus-summum-engineering-plus-edyta-augustynowicz-photo

Archello. (2024). *https://archello.com*. Retrieved from Archello: https://archello.com/fr/project/heydar-aliyev-center

ArchitectureCourses. (2024). *architecturecourses.org*. Retrieved from Hagia Sophia Architecture: https://www.architecturecourses.org/learn/hagia-sophia-architecture#:~:text=One%20of%20the%20most%20striking%20features%20of%20Hagia,to%20float%20effortlessly%20above%20the%20expansive%20interior%20space.

Banos, M. P. (n.d.). *Maqueta virtual para el cálculo estructural del oceanográfico de Valencia.* Universidad Politécnica de Cataluna Barcelona - Espana. Retrieved 2024, from https://upcommons.upc.edu/bitstream/handle/2099/16715/267_269%20PV10.pdf?sequence=1

Bensøe, M., & Sigmund, O. (1999). Material interpolation schemes in topology optimization. *Archive of applied mechanics 69*, pp. 635-654. doi:https://doi.org/10.1007/s004190050248

Berkel, J. v., Schoenaker, N., Steeg, A. v., Jongh, L. d., Schovers, R., Pieters, A., & Delahaye, R. (2019, September). *Centraal Bureau voor de statistiek.* Retrieved 2024, from www.cbs.nl: https://www.cbs.nl/nl-nl/publicatie/2019/45/materiaalstromen-in-nederland-2014-2016

Birch, C. P., Oom, S. P., & Beecham, J. A. (2007, August). Rectangular and hexagonal grids used for observation, experiment and simulation in ecology. *Ecological Modelling*(Issues 3-4), pp. 347-359. doi:https://doi.org/10.1016/j.ecolmodel.2007.03.041

BouwWereld. (2025). *Prefab Bouwen: de potentie van ee nbouwmethode-in-opkomst*. Retrieved from www.bouwwereld.nl: https://www.bouwwereld.nl/categorie/bouwtechniek/prefab/

Britannica. (2024). *Britannica.com*. Retrieved from Pantheon: https://www.britannica.com/topic/Pantheon-building-Rome-Italy

Britannica. (2024). *Dome of the Rock*. Retrieved from britannica.com: https://www.britannica.com/topic/Dome-of-the-Rock

BTAInternational. (2024). *Materieel en trailerafmetingen*. Retrieved from bta-international.com: https://www.bta-international.com/nl/informatie/afmetingen-vrachtwagens-trailers/

CBS. (2019, November). *Centraal Bureu voor de Statistiek*. Retrieved 2024, from www.cbs.nl: https://www.cbs.nl/en-gb/news/2019/45/construction-sector-leading-in-waste-and-recycling

Constar. (2024). *Betonplaten*. Retrieved from Constar.nl: https://constar.nl/betonplaten/?bg_source=bi&bg_source_id=71743397662164&bg_kw=kwd

-71743939966808:loc-129-pi-&bg_campaign=579041208&msclkid=8ae879d11a891a63246e1ed750a2ffb4&utm_source=bing&utm_medium=cpc&utm_campaign=(S)%20Betonplaten%20Constar&utm_term=b

Coster, A. D., Laet, L. D., & Tysmans, T. (2024). *Exploring the three-dimensional space with modular cocnrete shells: Form-finding, design and structural analysis.* Thin-Walled Structures, Volume 195. doi:https://doi.org/10.1016/j.tws.2023.111336

Coster, M., & Chermant, J.-L. (2002, August). On a way to material models for ceramics. *Journal of the European Ceramic Society*(Issue 8), pp. 1191-1203. doi:https://doi.org/10.1016/S0955-2219(01)00455-1

Das, R., Bhattacharya, I., & Saha, R. (2016). Comparative Study between Different Types of Formwork. *International Research Journal of Advanced Engineering and Science*(Issue 4), pp. 173-175. Retrieved from https://irjaes.com/wp-content/uploads/2020/10/IRJAES-V1N4P210Y16.pdf

Datta, B., & Maity, D. (2022, January). Platonic solids, Archimedean solids and semi-equivelar maps on the sphere. *Discrete Mathematics*(Issue 1). doi:https://doi.org/10.1016/j.disc.2021.112652

Davis, L., & Maïni, S. (2016). *Building with arches, vaults and domes: Training manual for achitects and engineers.* Auroville Earth Institute. Retrieved from https://wiki.opensourceecology.org/images/6/68/AVEI_building_with_arches_vaults_and_domes.pdf

Dede, T., Atmaca, B., Grzywinski, M., & Rao, R. V. (2020, August). Optimal design of dome structures with recently developed algorithm: Rao series. *Structures*, pp. 65-79. doi:https://doi.org/10.1016/j.istruc.2022.06.010

Dekeij. (2024). *Betonplaten prefab*. Retrieved from De Keij: https://www.dekeij.nl/betonplaten-prefab/

delinevietnam. (2015). *Deline Architecture & Construction, "Forest of meditation"*. Retrieved from https://delinevietnam.wordpress.com: https://delinevietnam.wordpress.com/2015/06/22/forest-of-meditation/

Dong, S., Nash, R. J., & Li, Y. (2024, August). Mechanical response of 3D printed irregular sutural tessellations with Voronoi tile patterns under tension. *Engineering Facture Mechanics*. doi:https://doi.org/10.1016/j.engfracmech.2024.110262

Fernhout, A. (2025, March). *Het belang en de mogelijkheden van duurzaam bouwen*. Retrieved from www.debeterewereld.nl: https://www.debeterewereld.nl/wonen-leven/het-belang-en-de-mogelijkheden-van-duurzaam-bouwen/

Fidelis. (2025). *First-Order vs. Second-Order Elements in FEA*. Retrieved from www.fidelisfea.com: https://www.fidelisfea.com/post/first-order-vs-second-order-elements-in-fea

Gaddam, M. S., & Achuthan, A. (2020). A comparative study on newly emerging type of formwork systems with conventional type of form work systems. *Materials Today: Proceedings*(33), pp. 736-740. doi:https://doi.org/10.1016/j.matpr.2020.06.090

Gawell, E., & Nowak, A. (2015). Voronoi tessellation in shaping the architectural form from flat rod structure. *PhD Interdisciplinary Journal*, pp. 47-55. Retrieved from https://www.academia.edu/31525486/Voronoi_tessellation_in_shaping_the_architectural_form_from_flat_rod_structure

Guan, Y., Virgin, L. N., & Helm, D. (2018, December 15). Structural behavior of shallow geodesic lattice domes. *International Journal of Solids and Structures*, pp. 225-239. doi:https://doi.org/10.1016/j.ijsolstr.2018.07.022

Harish, A. (2024, March). *What is convergence in Finite Element Analysis*. Retrieved from www.simscale.com: https://www.simscale.com/blog/convergence-finite-element-analysis/

Harish, A. (2024, March 11). *What is Convergence in Finite Element Analysis*. Retrieved from Simscale: https://www.simscale.com/blog/convergence-finite-element-analysis/

Hoogenboom, P. (2023, August). *CIEM5301 Shell Structures*. Retrieved from phoogenboom.nl: https://phoogenboom.nl/b17_schedule.html

Howison, M., & Séquin, C. H. (2019). CAD Tools for Creating Space-filing 3D Esher Tiles. *Computer-Aided Design and Applications*. doi:10.3722/cadaps.2009.737-748

iBouw. (2025). *De voor- en nadelen van prefab bouwen*. Retrieved from www.ibouw.nl: https://www.ibouw.nl/de-voor-en-nadelen-van-prefab-bouwen/

Jape, A. S., & Sayyad, A. S. (2023, December). A hyperbolic theory for the analysis of laminated shallow shells with double curvature. *Forces in Mechanics*. doi:https://doi.org/10.1016/j.finmec.2023.100246

Javan, A. R., Abdelaal, A., & Xie, Y. M. (2024, June). Creating 3D texture tessellation on planar surface using a single tile or a few tiles. *Frontiers of Architectural Research*. doi:https://doi.org/10.1016/j.foar.2024.05.001

Joneneel. (2024). *Betonplex*. Retrieved from Jongeneel.nl: https://www.jongeneel.nl/producten/plaatmateriaal/betonplex/c/W_24?q=%3Arelevance%3Alengte_mm%3A3000%3Abreedte_mm%3A1500

Karamba3D. (2024). *3.6: Algorithms*. Retrieved from https://manual.karamba3d.com: https://manual.karamba3d.com/3-in-depth-component-reference/3.5-algorithms/3.5.2-analyzethii

Kontovourkis, O., Phocas, M. C., & Katsambas, C. (2019). *Digital to physical development of a reconfigurable modular formwork for concrete casting and assembling of a shell structure.* Automation in Construction, Volume 106. doi:https://doi.org/10.1016/j.autcon.2019.102855

Kuo, S. (2023, August). Construction Archimedean tiling patterns based on soft materials from block copolymers and covalent organic frameworks. *Giant*. doi:https://doi.org/10.1016/j.giant.2023.100170

Lee, K. j., Danhaive, R., & Mueller, C. T. (2022, January). Spherical harmonic shape descirtors of nodal force demands for quantifying spatial truss connection complexity. *Architecture, Structures and Construction*, pp. 145-164. doi:https://doi.org/10.1007/s44150-022-00021-4

Li, W., Lin, X., Bao, D. W., & Xie, Y. M. (2022, April). A review of formwork systems for modern concrete construction. *Structures*, pp. 52-63. doi:https://doi.org/10.1016/j.istruc.2022.01.089

Liu, Y., Lee, T.-U., Javan, A. R., & Xie, Y. M. (2022, July). Extending Goldberg's method to parametrize and control the geometry of goldberg polyhedra. *Royal Society Open Science*. Retrieved from https://royalsocietypublishing.org/doi/epdf/10.1098/rsos.220675

Liu, Y., Lee, T.-U., Koronaki, A., Pietroni, N., & Xie, Y. M. (2023, March). Reducing the number of different nodes in space frame structures through clustering and optimization. *Engineering Structures*. doi:https://doi.org/10.1016/j.engstruct.2023.116016

Livinspaces. (2024). *https;//livinspaces.net*. Retrieved from Livinspaces: https://livinspaces.net/design-stories/projects/architecture/bosjes-chapel-south-africa-steyn-studio-tv3-architects/

Mahroo, H. A., & Vafamehr, M. (2023). Structural optimization of four designed roof modules: Inspired by Voronax grid shell structures. *Frontiers of Architectural Research 12*. doi:https://doi.org/10.1016/j.foar.2022.06.003

Marques, A. I., Morais, J., Morais, P., Veiga, M. d., Santos, C., Candeias, P., & Ferreira, J. G. (2020, Jarnuary 30). Modulus of elasticity of mortars: Static and dynamic analyses. *Construction and Building Materials*. doi:https://doi.org/10.1016/j.conbuildmat.2019.117216

Mohsin, F. (2024). *nl.pinterest.com*. Retrieved from Pinterest: https://nl.pinterest.com/pin/517843657158665873/

NEN-EN13670. (2009). *NENConnect.* Retrieved from https://connect.nen.nl: https://connect.nen.nl/Standard/PopUpHtml?RNR=149144&search=&Native=1&token=503a076c-e46b-419e-9b98-5a7449ce942d

Nuland, T. v., Dommelen, J. v., & Geers, M. (2021, January). An anisotropic Voronoi algorithm for generating polycrystalline microstructures with preferred growth directions. *Computational Materials Science*. doi:https://doi.org/10.1016/j.commatsci.2020.109947

Oesterle, S., Vansteenkiste, A., & Mirjan, A. (2012). Zero waste free-form formwork. *Proceedings of the Second International Conference on Flexible Formwork, Bath, United Kingdom*. Retrieved from https://www.academia.edu/66090147/Zero_Waste_Free_Form_Formwork

Oval, R. (2024). Nervi Puzzle: a topologically reconfigurable modular ribbed floor. *Proceedings of the IASS 2024 Symposium.* Zurich.

Rasheed, M., & Bajaj, C. (2015). Highly Symmetric and Congruently Tiled Meshes for Shells and Domes. *Procedia Engineering*, pp. 213-225. doi:https://doi.org/10.1016/j.proeng.2015.10.134

Sandra Gelbrich, H. L. (2018, October). Function-integrative textile reiforced concrete shells. *Open journal of composite materials*, pp. 161-174. doi:https://doi.org/10.4236/ojcm.2018.84013

Shakeri, S. (2022, February). *Sergio Musmeci, The Creator of Surreal Musmeci Bridge*. Retrieved from Pinterest: https://www.pinterest.ca/pin/300193131424433273/

Skrinar, M., & Plibersek, T. (2004, December). New linear spring stiffness definition for displacement analysis of cracked beam elements. *Proceedings in Applied Mathematics and Mechanics*(Issue 1), pp. 654-655. doi:https://doi.org/10.1002/pamm.200410308

Stevens, P., & Designboom. (2017, March). *designboom.com*. Retrieved from Steyn studio's bosjes chapel in south africa is crowned with a sculpptural roof canopy: https://www.designboom.com/architecture/coetzee-steyn-studio-bosjes-chapel-south-africa-sculptural-roof-canopy-03-13-2017/

TajMahal.gov. (2024). *Outlying Building*. Retrieved from tajmahal.gov.in: https://tajmahal.gov.in/outlying-building.aspx#:~:text=In%201632%2C%20the%20fifth%20Mughal%20Emperor%2C%20Shah%20Jahan%2C,an%20outer%20shell%20nearly%20200%20feet%20in%20height.

Tellier, X., Zerhouni, S., Jami, G., pavec, A. l., Lenart, T., Lerouge, M., . . . Baverel, O. (2020, March). The Caravel heX-Mesh pavilion, illustration of a new strategy for gridshell rationalization. *Discover*

Applied Sciences. Retrieved from https://link.springer.com/article/10.1007/s42452-020-2561-2

Tonelli, D. (2015, March). Statics Aware Voronoi Grid-Shells. *Thesis Universitá degli Studi di Pisa*. Retrieved from https://tesidottorato.depositolegale.it/handle/20.500.14242/130237

Tonelli, D., Pietroni, N., Puppo, E., Froli, M., Cignoni, P., Amendola, G., & Scopigno, R. (2016, June 1). Stability of Statics Aware Voronoi Grid-Shells. *Engineering Structures*, pp. 70-82. doi:https://doi.org/10.1016/j.engstruct.2016.02.049

Tumblr. (2009). *Meiso-no-mori crematorium & funeral hall by Toyo Ito and associates*. Retrieved from tumblr: https://theaccounts.tumblr.com/post/178119305/meiso-no-mori-crematorium-funeral-hall-by-toyo

Tyburec, M., Doskár, M., Zeman, J., & kruzík, M. (2022). Modular-topology optimization of structures and mechanisms with free material design and clustering. *Computer Methods in Applied Mechanics and Engineering 395*. doi:https://doi.org/10.1016/j.cma.2022.114977

Tyburec, M., Zeman, J., Doskár, M., Kruzík, M., & Leps, M. (2020). Modular-topology optimization with Wang tilings: an applicationi to truss structures. *Structural and Multidisciplinary Optimization 63*, pp. 1099-1117. doi:https://doi.org/10.1007/s00158-020-02744-8

UNEP. (2022, November). *www.unep.org*. Retrieved 2024, from UN environment progamme: https://www.unep.org/news-and-stories/press-release/co2-emissions-buildings-and-construction-hit-new-high-leaving-sector

VDMconstruction. (2024, October). *Lime Mortar vs Cement Mortar Key Differences*. Retrieved from www.vdmconstructions.com: https://www.vdmconstructions.com/construction/lime-mortar-vs-cement-mortar-key-differences/

Ventsel, E., & Krauthammer, T. (2001). *This Plates and shells, Theory: Analysis, and Applications* (1st ed ed.). CRC Press. doi:https://doi.org/10.1201/9780203908723

Verwimp, E., Tysmans, T., & Mollaert, M. (2013, September). Flexible formwork as reinforcement for curved concrete structures. *Proceedings of the International Association for Shell and Spatial Structures (IASS) Sympsium 2013*, pp. 1-10. Retrieved from https://www.researchgate.net/publication/275031346_Flexible_formwork_as_reinforcement_for_curved_concrete_structures

VisitVaticanCity. (2024). *VisitVaticanCity.com*. Retrieved from The Dome: https://www.visitvaticancity.org/monuments/saint-peters-basilica/the-dome/#:~:text=The%20Dome%20of%20St.%20Peter%27s%20Basilica%20with%20its,the%20basilica%2C%20of%20Rome%20and%20The%20Vatican%20City.

Wang, J., Gao, T., Li, M., Zhu, J., Song, L., & Zhang, W. (2024). Topology optimization of modular structures with multiple assemblies and applications to airborne shelves. *Chinese Journal of Aeronautics 37*, pp. 321-332. doi:https://doi.org/10.1016/j.cja.2023.12.014

Zhu, J. (2024, April). Optimisation Study of Building Structure Design Scheme based on K-means Clustering Algorithm. *Proceedings of the 2023 5th International Conference on Hydraulic, Civil and Construction Engineering (HCCE 2023)*. doi:https://doi.org/10.2991/978-94-6463-398-6_18